Received: 24 August 2021 | Revised: 8 December 2021 | Accepted: 28 January 2022

DOI: 10.1002/VIW.20210009

RESEARCH ARTICLE

Interactions between polymeric nanoparticles and different buffers as investigated by zeta potential measurements and molecular dynamics simulations

Wali Inam[1,2] | **Rajendra Bhadane**[1,3] | **Rukiye Nur Akpolat**[1,4] | **Rifahul Abrar Taiseer**[1] | **Sergey K. Filippov**[1] | **Outi M. H. Salo-Ahen**[1,3] | **Jessica M Rosenholm**[1] | **Hongbo Zhang**[1,2]

[1] Pharmaceutical Sciences Laboratory, Faculty of Science and Engineering, Åbo Akademi University, Turku, Finland

[2] Turku Bioscience Centre, University of Turku and Åbo Akademi University, Turku, Finland

[3] Structural Bioinformatics Laboratory, Faculty of Science and Engineering, Åbo Akademi University, Turku, Finland

[4] Department of Pharmacy, Ministry of Health, Alaca Public Hospital, Alaca, Corum, Turkey

Correspondence
Hongbo Zhang, Jessica M. Rosenholm, and Outi M. H. Salo-Ahen, Pharmaceutical Sciences Laboratory, Faculty of Science and Engineering, Åbo Akademi University, Biocity, 20520 Turku, Finland.
Email: hongbo.zhang@abo.fi; jessica.rosenholm@abo.fi; outi.salo-ahen@abo.fi

Funding information
Academy of Finland, Grant/Award Numbers: 328933, 336355, 337531; Sigrid Juséliuksen Säätiö (Sigrid Jusélius Foundation); Tor, Joe, and Pentti Borg Memorial Fund

Abstract

Zeta potential is an essential surface parameter in the characterization of nanoparticles, determined at the interface of loosely bound ions (diffuse layer) at the nanoparticle surface and free ions in solution. The ionic concentration and pH of the solution are known to, by definition, influence the composition of the diffuse layer and zeta potential accordingly. Thus, to fix the solution's pH for valid zeta potential measurements, buffers are frequently used. However, an issue that remains largely neglected is that buffers could also additionally alter the electrokinetic properties of nanoparticles through specific molecular interactions. Therefore, a thorough molecular understanding of buffer–nanoparticle interactions is needed to correctly implement zeta potential results. Thus, in order to study nanoparticle–buffer interactions, we first adopted a simple experimental approach of measuring zeta potential of common polymeric nanoparticle systems at different buffer concentrations, pH, and nanoparticle–buffer fraction ratios. We observed that zwitterionic/cationic buffer molecules impart significant interference to the electrokinetic properties of structurally diverse polymer nanoparticles, by causing zeta potential suppression or even inversion during the experiments. In parallel, advancement in computation resources nowadays allow studying intermolecular interactions of nanoparticles and other complex molecules by molecular dynamics (MD) simulations. Thus, by performing MD simulations for six different polymeric nanomaterials with commonly used buffer molecules, we found that noncovalent interactions play a significant role in altering the observed zeta potential values, which may contribute to erroneous results and false particle characterizations if not taken properly into account in zeta potential measurements.

KEYWORDS
buffer interaction, molecular dynamics simulation, polymeric nanoparticles, zeta potential

1 | INTRODUCTION

In pursuit of developing new nanoformulations, it is very pertinent to evaluate surface properties of nanoparticles to get insight into the colloidal stability of the formulation[1] and nanoparticle surface chemistry[2] under given conditions, which in turn determines the interactions of the nanosystem with the biological environment during application (a.k.a. the "nano-bio interface"). Thus, the electrostatic or charge repulsion/attraction between nanomaterials is one of the most fundamental parameters affecting the colloidal stability of nanoformulations,[3] and their interactions with their surroundings.[4] Nanoparticles, when dispersed in an ionic solution such as water, attain a surface charge, shielded by the layer of loosely bound counter ions, known as the diffuse layer. This allows the measurement of an important electrokinetic parameter, zeta potential, at the slipping plane that discriminates the diffuse layer from the free ions present in the solution. The distance extending between the layer of the firmly attached ions to the nanoparticle surface (or Stern layer) to the diffuse layer is known as the electrical double layer (EDL), as defined by Debye's parameter that is highly influenced by the ionic composition of the solution.[5] Therefore, zeta potential is required to be measured at a specific ionic concentration and pH. In this context, buffers are considered important media to characterize zeta potential of nanomaterials at a given pH. The general guidelines and principles governing the effect of buffer concentrations/pH on zeta potential are extensively discussed in the literature.[5,6] However, what has been largely ignored is that buffer molecules, through molecular interactions, could also alter the physicochemical and biological properties of nanoparticles and consequently, even the functionality of nanoparticles.[7] The situation is made even more complex in that nanoparticles used in nanomedicine seldom are "simple" materials i.e. made out of only one constituent, in order to render them functional in the first place. Besides the main material, every functional group, coating and/or functional moiety attached to the nanosystem may inflect a contribution to the acid/base properties of the overall system (and simultaneously, the surroundings) when immersed into an aqueous environment. Due to the usually quite complex acid/base properties of a nanosystem, tight buffering control of the solution is required when determining context-dependent properties such as zeta potential at a given condition for gaining a valid result.

The purpose of a buffer is thus to stabilise the formulations by regulating the consequential pH shift. However, if the buffer ingredients start interacting with the surroundings, they may induce favourable or unfavourable changes to the system.[8] 2-[4-(2-hydroxyethyl)piperazin-1-yl]ethanesulfonic acid (HEPES) is a zwitterionic molecule (pKa_1 ~3, sulfonic acid; pKa_2 7.55, basic piperazine nitrogen; effective buffer pH range 6.8–8.2) that is frequently used in biological experiments due to its buffering capacity at physiological pH. It has been shown that its two nitrogen atoms, for instance, allow it to adsorb on gold nanoparticle (AuNP) surfaces, which increases the colloidal stability of the particles. Therefore, adsorption of HEPES molecules prevents aggregation of AuNPs even at higher buffer concentration when compared to other buffer types.[9] On the other hand, HEPES–AuNP interactions unfavourably lowers the DNA detection sensitivity of AuNPs for colorimetric analysis.[10] Likewise, (tris(hydroxymethyl)aminomethane) (TRIS) buffer (pKa 8.08; effective buffer pH range 7–9), another common buffer used to mimic physiological conditions, and HEPES have shown to interact with titanium dioxide (TiO_2) surfaces and thus alter protein adsorption on mesoporous TiO_2 surfaces.[11]

The impact of molecular interactions with particle surfaces may even go beyond the material itself. For instance, it has been shown that the type of buffer solution can have a profound effect on the transfection efficiency of gene delivery vectors, due to the buffer molecules' specific interaction with the cationic polymer coatings.[7] Thus, functional groups and charge possessed by buffer molecules play an important role in determining the interaction of buffers with different materials. Given the fact that buffers and electrolytes could interfere with their surroundings, it is likely that buffers may also influence the surface properties of nanoparticles such as zeta potential. Therefore, selecting a buffer molecule among the range of available buffers for zeta potential determination of nanoparticles could pose a challenge that needs a thorough molecular understanding.

In the quest of studying buffer interactions with colloidal systems, most of the studies have focused on inorganic nanomaterials while organic materials have not been explored in similar capacity.[10] Consequently, there is no specific method that could ensure the selection of a correct buffer system for evaluation of organic nanoparticle formulations. Polymers are increasingly used to develop highly functional nanoparticles

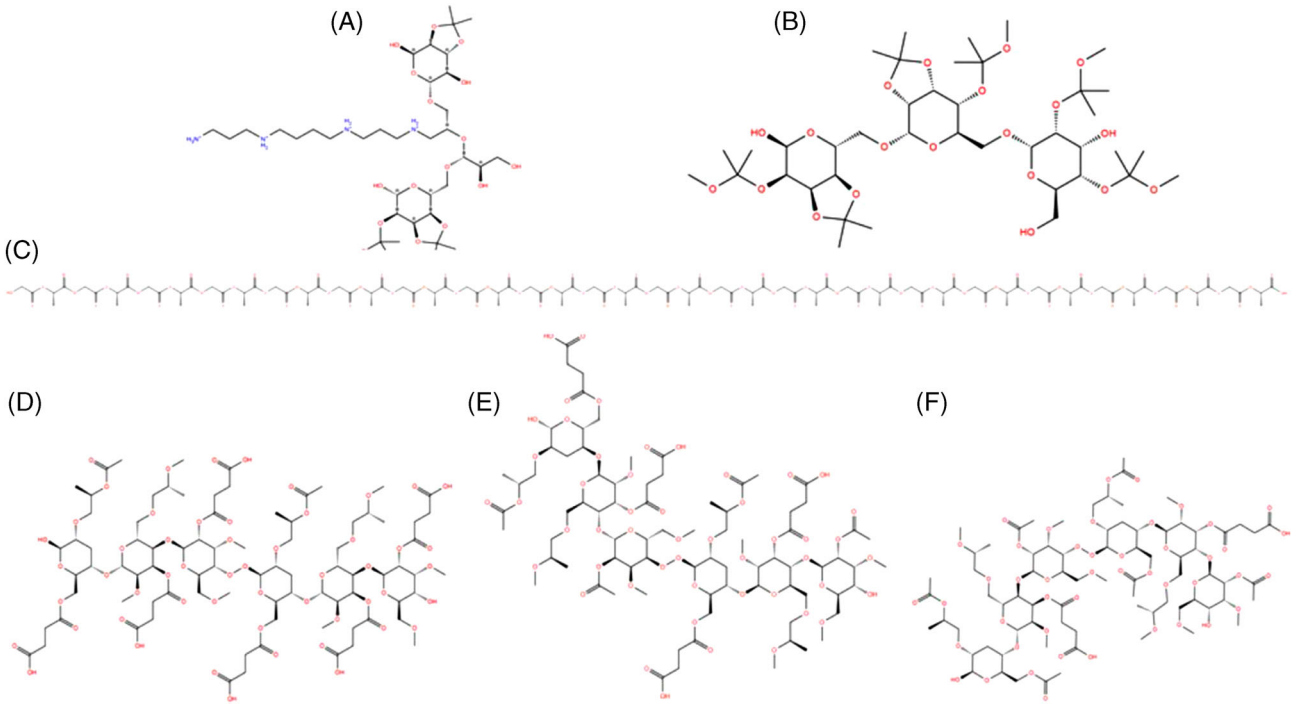

FIGURE 1 2D structures of the polymers used in this study. (A) SpAcDEX, (B) AcDEX, (C) PLGA, (D) HPMCAS-HF, (E) HPMCAS-MF, and (F) HPMCAS-LF

e.g. for on-demand and controlled drug delivery systems.[12]

The polymer compositions are precisely engineered to tune the polymer chemistry for creating conjugation possibilities and attributing intuitive properties (swelling, degradation) to polymeric particles.[13] Recently, acetalated dextran (AcDEX) and spermine modified acetalated dextran (SpAcDEX) polymeric platforms were synthesized as pH responsive materials that were shown to hydrolyse at acidic pH, rendering them highly interesting for intracellular delivery. Both polymers share a similar dextran ring; however, the former expresses hydroxyl moieties (anionic/acidic), whereas the latter has an additional polyamine chain (cationic/basic).[14,15] In addition, the US Food and Drug Administration (FDA) has approved poly(lactic-co-glycolic acid) (PLGA) polymers that are slowly hydrolysed in the presence of water for drug delivery applications.[16,17] Another polymer of pharmaceutical interest, hydroxypropyl methylcellulose acetate succinate (HPMCAS) is available in three grades, that is, HPMACS-HF, HPMCAS-MF, and HPMCAS-LF, produced, which is modified by the variation of succinyl (∼6%, ∼11%, and ∼12%) and acetyl (∼12%, ∼9%, and ∼6%) content.[18] These polymeric materials have great structural diversity, which makes them an interesting platform to study polymer–buffer interactions. Structures of the polymers studied in this study are shown in Figure 1.

To study electrokinetic properties of nanoparticles fabricated from structurally diverse polymer materials, the process of nanofabrication needs to be optimized so as to obtain nanoparticles (differing in their chemical composition) resembling in size, shape, and polydispersity. These critical physiochemical parameters could influence the electrophoretic mobility of particles that could consequently affect the zeta potential.[19,20] To achieve the uniformity in the particle fabrication process, particle synthesis could be materialised in a confined and controlled environment of miniature microfluidic device. The microchannels of microfluidics permit fast diffusion, even mixing of solvents and rapid precipitation thus particles produced are monodisperse and possess small size. Moreover, controlled fluid flow dynamics of microfluidics ensure method reproducibility.[21] Further, after proper washing of microfluidics channels same device could be reused, thus single microfluidics device could serve as a platform to fabricate particles from various polymer materials. To this advantage of microfluidics, in this study, we used coaxially arranged glass capillaries as a microfluidics platform for fabricating nanoparticles from six different polymer materials that were latter used to study polymer–buffer interaction through zeta potential measurement.

Complementary to the experimental methods, the application of computational simulations in formulation development is gaining increasing interest.[22] The

significant increase in current computational power has made it possible to perform atomic-level molecular simulations of nanoparticles and other molecularly complex formulations.[23–25] Since the size of the nanoparticles utilized for drug delivery purposes typically ranges from 50 to 500 nm,[26] simulating this large structures for a few nanoseconds may be challenging, depending on how much computational power is available. Nevertheless, it is possible to speed up the simulations by using only the model of the interfaces and ignoring the core part of the nanoparticles. Likewise smaller molecules (drugs or buffers) can be modeled and simulated along with the structural models of polymer nanoparticles. Molecular simulations can then be used to predict the dynamics of molecular interactions between the different entities in the simulation system.

Interactions between the ionic species in the bulk solution and at the nanoparticle interface are usually studied through special spectroscopic techniques such as electron paramagnetic resonance spectroscopy[27] or X-ray photoelectron spectroscopy.[28] However, here we rather adopted a simple approach of measuring zeta potential of nanoparticles prepared from the organic polymers AcDEX, SpAcDEX, PLGA, HPMCAS-HF, HPMCAS-MF, and HPMCAS-LF as a function of ionic strength, pH, and the nanoparticle–buffer fraction ratio; in order to predict changes perturbed at the nanoparticle surface due to nanoparticle–buffer interactions. Additionally, we used molecular dynamics (MD) simulations to get atomic-level understanding on buffer–nanoparticle interactions to better explain our experimental data. We foresee this study to constitute an important guide in the correct selection of measurement conditions in zeta potential measurements involving polymeric nanoparticles for applications within nanomedicine.

2 | METHODS

2.1 | Fabrication of nanoparticles

2.1.1 | AcDEX and SpAcDEX nanoparticles

For synthesis of AcDEX and SpAcDEX nanoparticles similar protocol was followed. Briefly, 10 mg of polymer (AcDEX/SpAcDEX) was dissolved in 4 ml of ethanol (Ethax, 99.5%) to make a final concentration of 2.5 mg/ml. Aqueous solution 0.1% Pluronic F127 (sigma) with pH adjusted to 7.5 ± 0.2 was used as counter solvent. Polymer solution and counter solvent were infused in the inner and outer capillary of the glass capillary microfluidics chip at the flow rate of 2 ml/h and 40 ml/h, respectively with aid of two Harvard pumps (PHD 2000, Harvard Apparatus, USA). Nanoparticles collected were analysed with Zetasizer nano ZS (Malvern) and TEM (JEM-1400 Plus Electron Microscope, JEOL, Japan).

2.1.2 | PLGA nanoparticles

PLGA nanoparticles were fabricated by using nanoprecipitation method with aid of microfluidics platform. PLGA was weight upto 10 mg and dissolved in 5 ml of acetone (Sigma, HPLC grade) to make a final concentration of 2 mg/ml. PLGA and aqueous solution (0.1% Pluronic F127, pH 7.5 ± 0.2) were infused in the outer capillary and simultaneously focused on the inner capillary. PLGA and aqueous solution were set to the infusion rate of 2 ml/h and 20 ml/h. Nanoparticles were collected for analysis.

2.1.3 | HPMCAS (LF, MF, and HF) nanoparticles

HMPCAS (HF, MF, and LF) polymers were provided by the Helsinki University. To fabricate particles, polymer solution (2.5 mg/ml) was prepared in acetone and pumped in the inner capillary at 2 ml/h and precipitated with Milli Q (pH 4) flown at the rate of 40 ml/h in the outer capillary. Nanoparticles were collected in glass vial at outlet of the chip for analysis.

2.2 | Characterization

2.2.1 | Dynamic light scattering (DLS)

Hydrodynamic size of nanoparticles was characterized with dynamic light scattering instrument, Zetasizer Nano ZS. Sample preparation was done by dispersing 200 μl of nanoparticles from stock suspension of polymeric nanoparticle to the 1 ml of deionized water (DI), which was filtered prior with 450 μm acrodisc filter. Sample was sonicated and vortexed alternatively for 2 min and transferred to disposable cuvettes and placed in the sample holder of the instrument.

2.2.2 | TEM characterization

Prior to preparing TEM samples, polymer nanoparticles were washed with a specific solvent, once by successively centrifugation, vortexing, and sonication. DI water (pH 8) was used to wash AcDEX, SpAcDEX nanoparticles; HMPC (HF, MF, and LF) nanoparticles were washed with DI water (pH 4); and PLGA was washed with simple DI water. TEM grids were prepared by dropping 10 μl dilute dispersion of each nanoparticle preparation on copper grid and

kept it for drying overnight. Images of particles were taken with JEM-1400 Plus Electron Microscope.

2.2.3 | Zeta potential measurement

Zeta potential of nanoparticles was measured using Zetasizer Nano ZS (Malvern). Each dispersion containing 1–60 μg of particles was carefully filled in disposable folded capillaries (Malvern) to avoid bubbling. Disposable folded capillary was placed in the instrument for taking measurements. The zeta potential, as a function of particles/HEPES fraction ratio, buffer pH and buffer concentration was measured at least thrice. The final zeta potential was calculated by taking average of three values and reported along with the standard deviation (shown as the error bars in Figures 5–7). After measurements, disposable folded capillary cells (Malvern) were washed with DI water/ethanol and dried by blowing air. Whereas electrodes of disposable folded capillary were monitored continuously and replaced by the new ones if blackening was observed.

2.3 | Computational studies

2.3.1 | Polymer preparation

To obtain representative models of nanoparticles under investigation and to understand polymer–buffer interactions at the interface, atomic scale models of polymers were prepared ignoring the noninteracting core of nanoparticles. The structures of the initiator and terminator end groups of polymers were sketched using the Polymer Builder tool of Schrödinger's Material Science suite release 2021–2022 (Schrödinger, LLC, New York, NY, 2021). To build the polymer chains, monomers of all these polymers were built as shown in Figure 1. The backbone dihedral angle was set to random. The clashes between C-C and C-H atoms were avoided by specifying the van der Waals scale factor of 0.50 with a random seeding option.

2.3.2 | Simulation system preparation

To prepare a simulation system with a set number of polymers and buffer molecules with or without water molecules, the Disordered System Builder panel of the Schrödinger Material Science suite was used. The maximum number of polymer chains in each system was 20. Each system had an initial density of 0.5 g/cm^3 and periodic boundary conditions (PBC) with an orthorhombic unit cell were used for all simulations. The initial disordered system was set to a "tangled chain" using the OPLS4e force field.[29] The 2D structures of the HEPES and TRIS were sketched with the 2D Sketcher tool in Maestro and processed further to 3D structures using the LigPrep tool of Schrödinger's Maestro molecular modelling suite (LigPrep, Schrödinger, LLC, New York, NY, 2021).

2.3.3 | Molecular dynamics simulations

The polymer and the copolymer with buffer molecules with and without water molecules were submitted to a 100-ns molecular dynamics (MD) simulation. The simulation was performed using the multistage MD simulation workflow of Desmond (Schrödinger Release 2021–2022: Desmond Molecular Dynamics System, D. E. Shaw Research, New York, NY, USA, 2021; Maestro-Desmond Interoperability Tools, Schrödinger, New York, NY, USA, 2021),[30] consisting of a three-stage material relaxation protocol, followed by a 100-ps Brownian dynamics (BD) simulation, and finally the production MD simulation and analysis. Briefly, the material relaxation protocol involved 20 ps of Brownian dynamics (BD) at 10 K to remove steric clashes, followed by a short BD simulation at 100 K in the NPT ensemble and an anisotropic coupling scheme. In the final stage, a 100-ps MD simulation in the NPT ensemble was completed using anisotropic coupling and a 2-fs time step. The production simulation was then performed for 100 ns at 300 K and 1.01325 bar with the Nose-Hoover chain thermostat[31–33] and barostat using the Martyna-Tobias-Klein method[34] with isotropic coupling. The Coulombic method used for long-range interactions was U-series[35] while the cut-off radius for short-range interactions was set to 9.0 Å. Various bulk properties derived from the simulation trajectories were calculated using the Simulation Event Analysis panel of the Schrödinger Material Science suite. The hydrogen bonding interactions were further analysed in Microsoft Excel360.

3 | RESULTS

3.1 | Nanoparticle fabrication and characterization

Polymeric nanoparticles were fabricated with the aid of microfluidics using a coaxially arranged glass capillary, assembled on the glass slide as a microfluidics chip. In brief, polymer solution was propelled through the inner capillary, which was focused into a narrow stream with the aid of aqueous solution (0.1% Pluronic F127 [pH 7.5 ± 0.2]/distilled water pH 4) flown in the outer capillary. The nanoprecipitation-based fabrication of nanoparticles was materialized due to the difference in solubility of polymer in organic solvent and counter solvent (0.1% Pluronic F127 [pH 7.5 ± 0.2]/distilled water pH 4). Hydrodynamic size

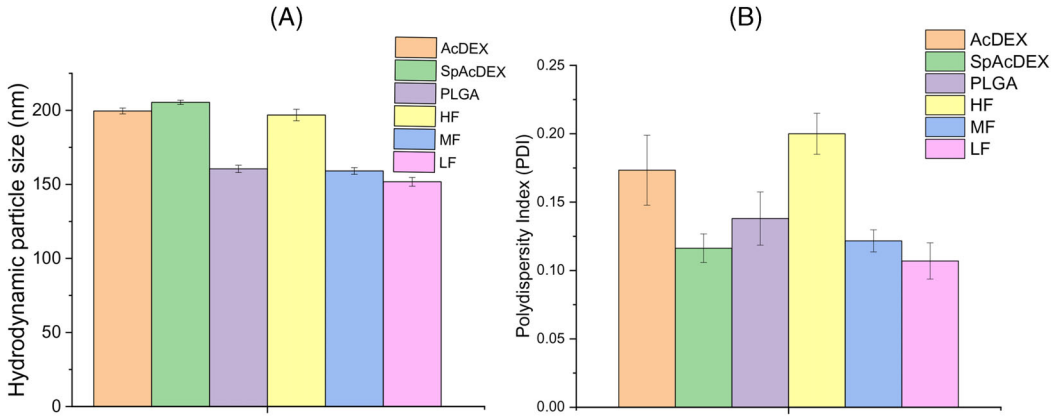

FIGURE 2 Characterization of nanoparticles (AcDEX, SpAcDEX, PLGA, HPMCAS LF, MF, HF) by DLS. (A) Bar chart shows the hydrodynamic size of the nanoparticles, calculated as average Z-diameter and (B) polydispersity index

and polydispersity index (PDI) measurements were taken in triplicate and hydrodynamic particle size was calculated by taking Z-average values and reported along with standard deviations (Figure 2). For more detailed characterization of the nanoparticles' morphology, particles dried over a copper grid were imaged using TEM microscopy. Area of the particles of each polymer was analysed with Image J, and the data obtained was converted to obtain the particle diameter by using simple $A = \pi r^2$ formula defining the dimensions of a sphere.

3.1.1 | SpAcDEX and AcDEX nanoparticles

For fabricating small and monodispersed nanoparticles from AcDEX and SpAcDEX, concentration of respective polymers was adjusted to 2.5 mg/ml, and polymer solution was flown in the inner capillary at 2 ml/h and consequently counter solvent (0.1% Pluronic F127, pH 7.5 ± 0.2) was propelled in the outer capillary at 40 ml/h. Neutral pH was maintained to prevent hydrolysis of acetal groups associated with AcDEX and SpAcDEX polymers. The hydrophobicity of the polymers (AcDEX and SpAcDEX) allows quick precipitation upon exposure to the aqueous solution. DLS result showed that AcDEX and SpAcDEX particles had a hydrodynamic particle size of 199.5 ± 1.97 nm and 205.4 ± 1.49 nm, respectively (Figure 2B). Moreover, the particles exhibited low polydispersity index (PDI) values (<0.2; Figure 2B) and possessed narrow size distribution (see Supplementary information Figure S1). In TEM microscopy, AcDEX and SpAcDEX particles appeared as condense spherical particles (Figure 3A and B). Image analysis showed that the average diameter of AcDEX and SpAcDEX was 150 ± 5 and 123.2 ±33.88 nm, respectively. The difference in the particle size values between DLS and TEM is due the difference in the working principle of the two techniques. In the former, measurements are carried out in the solution where a cloud of ionic species envelop the particle leading to increase in the hydrodynamic size of the particle. Contrarily, in TEM microscopy particles, imaging is done in dried state. Further, DLS technique relies on light scattering data, which are easily influenced by the presence of particle aggregation and agglomeration. It has been shown that light scattering cross-section could potentiate to as high as 1000-fold upon switching the particle size from 30 to 80 nm.[36] Hence, particle size estimated with DLS was high as comparison to TEM, as expected.

3.1.2 | PLGA nanoparticles

The synthesis of PLGA nanoparticles was optimized by carefully selecting the polymer concentration, solvent system, and flow rate. Literature shows that size and polydispersity of PLGA particles is highly influenced by the concentration of polymer and selection of organic solvent system.[37,38] Keeping in view the concentration range 1–40 mg/ml used in the literature, we prepared 2 mg/ml of PLGA solution in acetone and propelled through the inner capillary of microfluidics chip at 2 ml/h whereas outer capillary was supplemented with 0.1% Pluronic F127, pH 7.5 ± 0.2 at the flow rate 20 ml/h. The aqueous solution used in outer capillary caused precipitation of hydrophobic PLGA whereas surfactant (Pluronic F127) served as a stabilizer. DLS result showed that PLGA particles had a hydrodynamic particle size of 160 ± 2.48 nm with small PDI 0.14 ± 0.02 (Figure 2A and B). Size distribution curve suggested that PLGA particles possess narrow size distribution (see Supplementary information Figure S1). According to the TEM images, PLGA particles has spherical shape and appear less dense in comparison to the other particles (Figure 3C). This could be due to the dominance of loosely arranged brush hair-like structures of PLGA molecules at

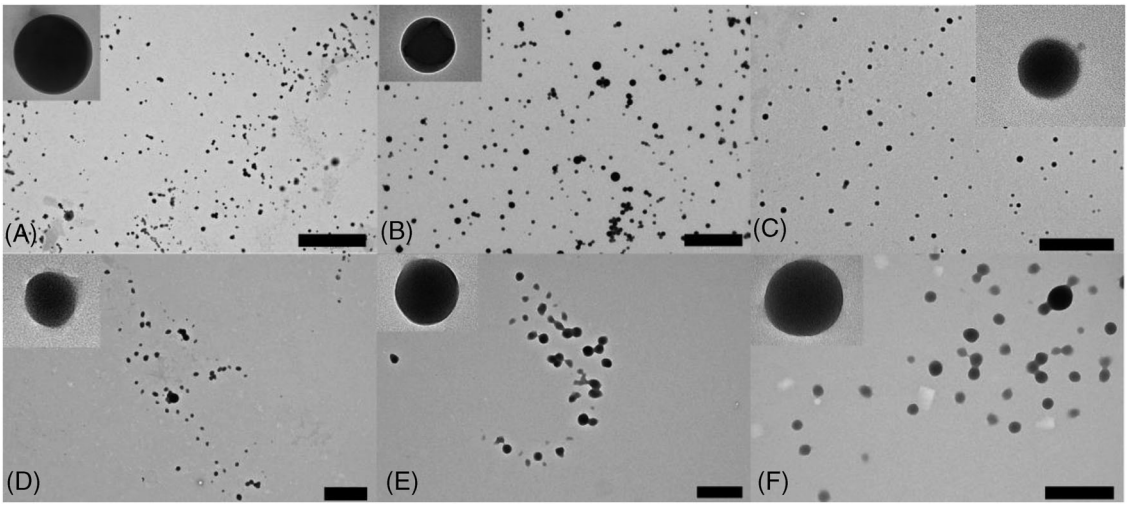

FIGURE 3 Micrographs of the fabricated particles. (A) Acetalated dextran (AcDEX); scale bare 5 μm. (B) Spermine modified acetalated dextran (SpAcDEX); scale bar 200 μm. (C) Poly(lactic-co-glycolic acid) (PLGA): scale bar 200 μm. (D) Hydroxypropylmethylcellulose acetate succinate (HPMCAS)-LF; scale bar 1 μm. (E) HPMCAS-MF; scale bar 500 μm. (F) HPMCAS-HF; scale bar 500 μm, acquired by transmission electron microscope (TEM)

the periphery, which allows the electron beam to transmit, pertaining to lower density of PLGA particles. Analysing TEM images of PLGA particles showed that the average diameter of PLGA particles was 111 ± 55.0 nm, which was lower than the hydrodynamic particle size from DLS. Again, the difference in the results could be attributed to the presence of possible aggregates and presence of molecular ionic envelope around the particle.

3.1.3 | HPMCAS (HF, MF, and LF) nanoparticles

Owing to the hydrophobic nature, acetone was selected as a common solvent for all three grades of HPMCAS (HF, MF, and LF). Precipitation of polymer solution was triggered at 2.5 mg/ml concentration by exposing to pH 4 deionized water at the flow rate of 40 ml/h. HPMCAS solubility is influenced by chemical modifications, changing the ratio of acetyl and succinyl functional moieties solubility of HPMCAS could be triggered from pH 5.0 to 6.8. Since HPMCAS-HF, HPMCAS-MF, and HPMCAS-LF are stable in acidic environment, particles were fabricated under slightly acidic aqueous environment. DLS result showed that hydrodynamic particle size of HPMCAS-HF, HPMCAS-MF, and HPMCAS-LF was 196.8 ± 3.9, 159.1 ± 2.28, and 151.7 ± 2.95 nm (Figure 2A), respectively. The PDI values were found in lower range 0.13 ± 0.08, 0.12 ± 0.01, and 0.11 ± 0.01 for HPMCAS-HF, HPMCAS-MF, and HPMCAS-LF, respectively (Figure 2B). Further, TEM microscopy showed that the HPMCAS-HF, HPMCAS-MF, and HPMCAS-LF have spherical morphology (Figure 3D–F) and have an average particle size of 88.87 ± 26.84, 111.32 ± 32.44, and 99.57 ± 26.75 nm, respectively. Based on the DLS and TEM microscopy data, it was affirmed that all polymer particles synthesized have spherical morphology that complies with the assumptions made by Smoluchowski and Henry.[39,40] Further, polymer particles have comparable particle size as well as narrow size distribution (see Supplementary information Figure S1) and are hence suitable for zeta potential investigation.

3.2 | Evaluating zeta potential of polymer nanoparticles and HEPES fractions ratios

Different fraction ratios of polymer nanoparticles and HEPES were prepared by mixing alternating volumes of respective components. By preparing different fraction ratios (Fr), it was possible to observe changes in zeta potential, which might result due to interaction of particles and HEPES, while the pH of the system was kept relatively constant (±0.1). To formulate the highest fraction ratio (Fr_H, 19) 2.85 μl of nanoparticles (80–150 μg) were mixed with 150 μl HEPES (25 mM), diluting HEPES to 1.3 mM. Subsequently, zeta potential and pH of the particle dispersion were measured. In the following experiment, fraction ratio (Fr) was reduced by adding more HEPES to increase buffer concentration to 2.5, 10, 18.7, 22.5, and 25 mM, respectively; in contrast, nanoparticles were depleted from the system. Overall concentration of particles was altered from 180 to 0.1 μg. Zeta potential and pH measurements were taken for all dispersion systems prepared as a fraction ratio. Thus, alternatively changing nanoparticle and buffer concentration aided us to follow changes at the nanoparticle surfaces due to interaction of buffer molecules.

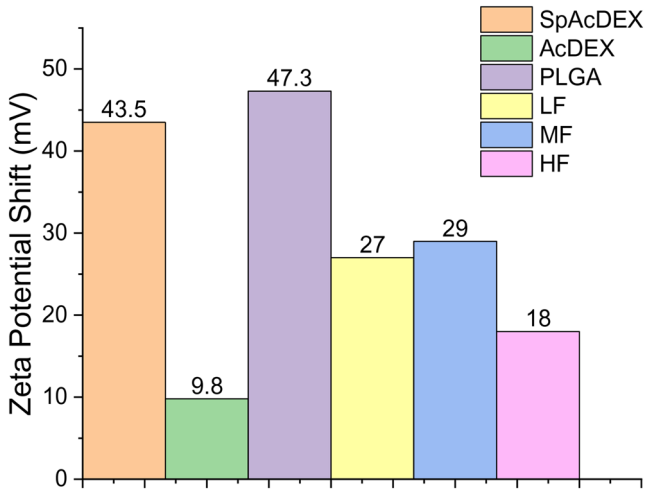

FIGURE 4 Zeta potential shifts are plotted as bar charts showing the difference of zeta potential between lowest and higher fraction ratio (particles/HEPES). SpAcDEX (pH 7.2 ± 0.1), AcDEX (pH 7.2 ± 0.1), PLGA (pH 7.4 ± 0.1), and HPMCAS (HF, MF, LF ; pH 4 ± 0.1)

3.2.1 | HEPES and SpAcDEX/AcDEX nanoparticles

SpAcDEX particles showed zeta potential of 29.5 mV at highest fraction ratio (Fr_H, 19, HEPES 1.3 mM, pH 7.1; Figure 5). The high positive zeta potential appeared due to the presence of polyamine chain (spermine) linked with the dextran backbone chain as shown in Figure 7. Upon decreasing the Fr, zeta potential dropped gradually and flipped to –14.2 mV at the lowest fraction ratio (Fr_L) 0.002 (HEPES 25 mM, pH 7.2; Figure 5). Since the pH of the system was kept relatively constant, changes in zeta potential could be assumed to result from interaction between HEPES and nanoparticles due to alternative change in concentrations of the respective components.

The expression of negative zeta potential (–14.2 mV) at the lowest fraction ratio (Fr_L) 0.002 (HEPES 25 mM, pH 7.2) by SpAcDEX particles bearing polycationic chain (spermine) and lacking any anionic moiety was an unexpected phenomenon, which alsostemmed an overall shift in zeta potential of 43.5 mV between Fr_L (0.002, HEPES 25 mM, pH 7.2) and Fr_H (19, HEPES 1.3 mM, pH 7.1) as shown in Figure 4. This trend in zeta potential shift depicts some prominent change occurring at the interface of the nanoparticle surface and Stern layer that could result from the molecular interaction of HEPES with the nanoparticle brush hairs.

Alternatively, zeta potential of different fraction ratios of polycation lacking AcDEX nanoparticles/HEPES were also evaluated. We observed that HEPES (150 μl, 1.3 mM) at Fr_H (19) could not keep pH of the system constant and hence we excluded results obtained from Fr_H (19). Analysing the trend of zeta potential from Fr 9 to 0.002, we observed that zeta potential continuously declined from –11.5 mV (HEPES 2.5 mM, pH 7.1) to –3.9 mV (HEPES 25 mM, pH 7.2) as shown in Figure 5. Descending Fr from highest to lowest prompted an overall zeta potential shift of only 9.8 mV (Figure 4). The appearance of negative potential shows the presence of acidic hydroxyl groups associated with dextran moiety.

In comparison to AcDEX, a sublime shift in zeta potential (43.5 mV) of SpAcDEX particles under relatively constant pH (7.2 ± 0.1) and overall small buffer concentration range (1.3 and 25 mM), and exhibition of zeta potential flipping behaviour observed at lower Fr gives evidence that electrokinetic properties of SpAcDEX particles are significantly altered under varying fraction ratios (particles/HEPES). From the structural standing, it is speculated that nitrogen containing polycationic chain (spermine) could specifically interact with the sulfonic acid moiety of the HEPES molecule. This could facilitate HEPES to adsorb at the particle surface (particularly under access of HEPES) thus altering surface chemistry by capping the basic functional moieties (polycationic, spermine chain) at the surface of SpAcDEX particles. Thus, interaction between SpAcDEX particles and HEPES might play a significant role in causing unexpected shift in zeta potential of SpAcDEX particles, which is not observed in AcDEX particles.

3.2.2 | HEPES and PLGA nanoparticles

In the similar manner as above, PLGA particles and HEPES fraction ratios were prepared, and zeta potential and pH measurements were performed. PLGA particles mixed with HEPES (1.3 mM) at Fr_H (19) at pH 7.2) showed high negative zeta potential –58 mV (see Figure 5). When Fr was decreased, consequently the zeta potential also declined and lowest zeta potential of –11.4 mV was recorded at Fr 0.002 (HEPES 25 mM, pH 7.4) as shown in Figure 5. We did observe a slight change in pH while HEPES was diluted from 25 to 1.3 mM, though. However, this change in pH is relatively insignificant in comparison to an overall sublime zeta potential shift (47.3 mV) exhibited by PLGA particles as shown in Figure 4. The possible interaction between HEPES and PLGA particles surface might be responsible for this significant shift in zeta potential. HEPES containing the piperazine ring bears two nitrogen atoms that could possibly interact with terminal carboxylic ends expressed on the surface of PLGA particles, thus capping and supressing the anionic character of the PLGA particles under access of buffer.

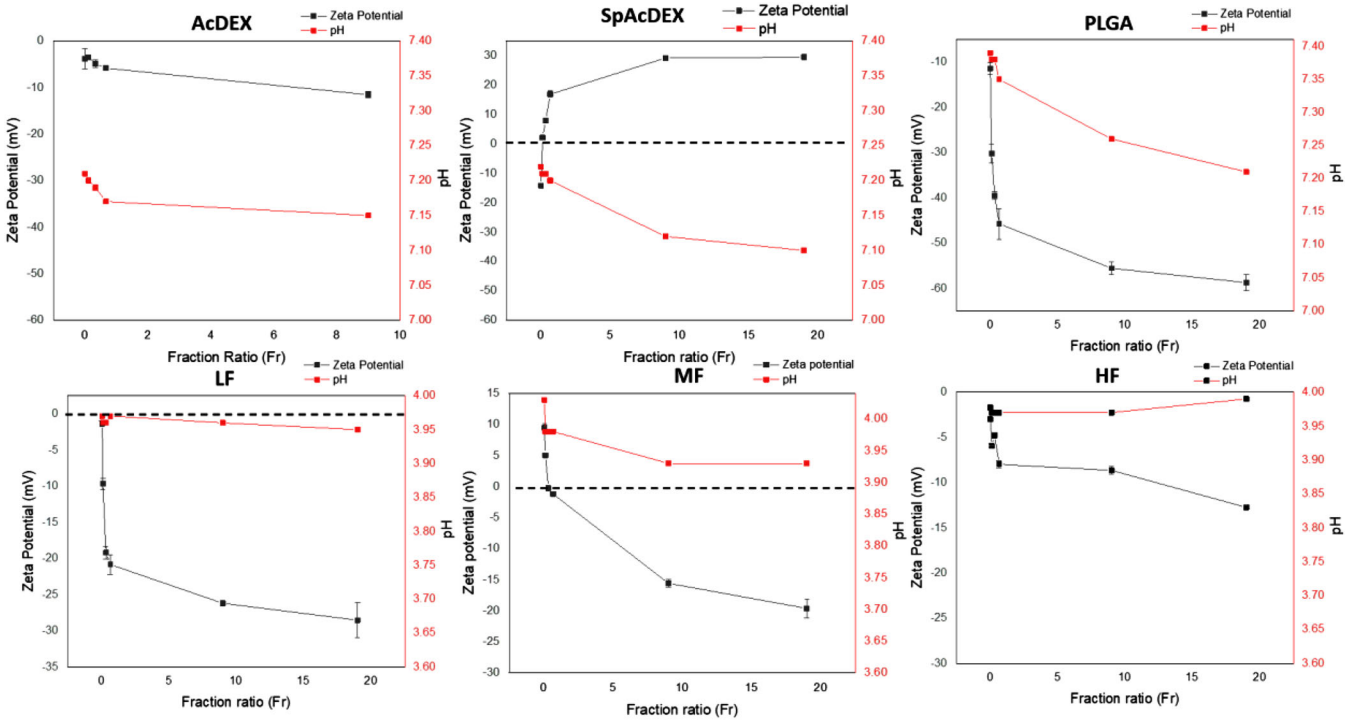

FIGURE 5 Zeta potential of polymer particles plotted as a function of fraction ratio (Fr) ranging from 0.002 to 19. In all experiments, HEPES buffer concentration was changed from 25 to 1.3 mM from lowest to highest fraction ratio, and consequently the particle concentrations were altered from 0.1 to 180 μg. The pH of nondiluted HEPES buffer was 7.2 for SpAcDEX, AcDEX; 7.4 for PLGA; and 4 for HPMCAS-HF, HPMC-MF, and HPMC-LF. Zeta potential of each Fr was measured with Zetasizer Nano ZS. Dotted line is drawn to denote zero zeta potential, and error bars represent standard deviation as calculated from the three measurements

3.2.3 | HEPES and HPMCAS nanoparticles

Similarly, we also investigated HPMCAS particles comprised cellulose backbone linked with functional groups (methoxy, acetyl, and succinyl). Acetyl and succinyl content of HPMCAS is modified in order of ~12–6% and ~6–12% to get three grades HPMCAS-HF, HPMCAS-MF, and HPMC-LF.[18] The succinate group associated with HPMCAS has pKa ca 4 as predicted by Epik, thus bears acidic character (see Supplementary Information Table S1). Faction ratios of different grades of HPMCAS and HEPES were also evaluated to analyse the impact of complex surface chemistry of polymers on zeta potential of respective nanoparticles. At Fr_H 19 (HEPES 1.3 mM, pH 3.9) HPMCAS-LF, MF and HF particles exhibited zeta potential of –28.5, –19.6, and –12.7 mV, respectively as shown in Figure 5. The expression of negative zeta potential values was expected, as the surface of HPMCAS particles is occupied by the acidic succinate groups. However, the zeta potential at Fr_H 19 (HEPES 1.3 mM, pH 3.9) was also found to correlate with the amount of succinyl content on three HPMCAS grades (LF > MF > HF). Zeta potential of HPMCAS particles declined as the Fr was decreased. Zeta potential of HPMCAS-HF and HPMCAS-LF was suppressed to –1.7 and –1.3 mV, respectively, at Fr_L 0.002 (HEPES 25 mM, pH 3.9; Figure 5). However, HPMCAS-MF showed slight positive zeta potential 9.5 mV at Fr_L 0.002 (HEPES 25 mM, pH 3.9; Figure 5). Furthermore, HPMCAS-LF, HPMCAS-MF with more succinyl content showed an overall shift in zeta potential of 27 and 29 mV, respectively, whereas HF with lowest succinyl content 18 mV shift in zeta potential (Figure 4). It is noteworthy that the shift in zeta potential of all HPMCAS particles is considerably less as compared to carboxylic acidic bearing PLGA polymer, probably because PLGA terminal carboxylic moieties (ca pKa 3) possess more acidic nature as compared to succinyl moiety (ca pKa 4) of HPMCAS (see Supplementary Information Table S1). The zeta potential shift of all six particles is shown in Figure 4.

3.3 | Zeta potential as a function of buffer concentration: comparison between HEPES and TRIS

One of the key roles of buffers is to provide sufficient ionic concentration to build up a diffuse layer around the nanoparticle for correctly evaluating zeta potential.

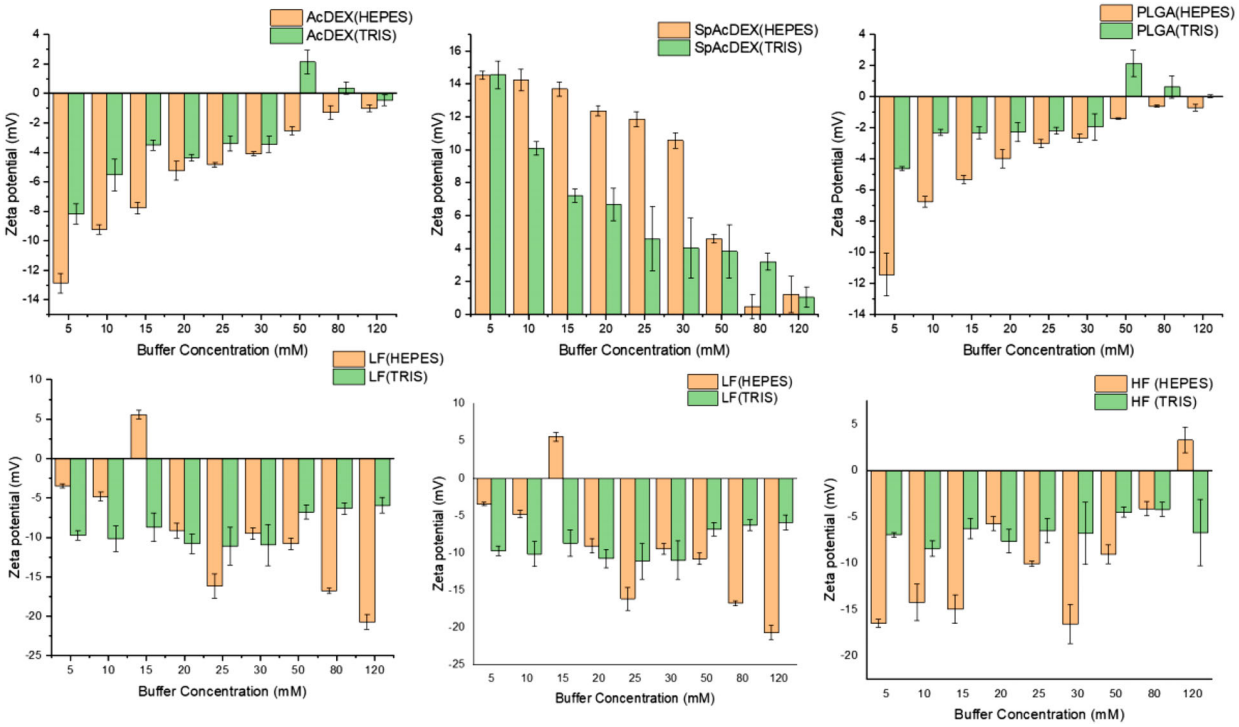

FIGURE 6 Zeta potential as a function of concentration of HEPES and TRIS at constant pH. AcDEX, SpAcDEX and PLGA were buffered at pH 7, whereas HPMCAS-HF, MF, and LF particles were buffered at pH 4. Error bars represent standard deviation as calculated from the three measurements

However, if in doing so, buffer molecules start to interact with the nanoparticle surface, this could disrupt the electrokinetic properties of the colloidal system. To foresee possible interference of buffers with nanoparticle's electrokinetic behavior such as zeta potential, we compared the zeta potential of polymer nanoparticles over a concentration range of 5–120 mM of HEPES bearing cationic center consisting of two nitrogen atoms and one anionic sulfonic acid moiety, whereas TRIS was used as a model molecule containing single nitrogen atom (cationic center). AcDEX, PLGA, and SpAcDEX particles (concentration ranging from 3 to 10 μg) were buffered at pH 7.4, whereas HMPCAS-LF, HMPCAS-MF, and HMPCAS-HF (concentrations ranging from 3 to 6 μg) were buffered at pH 4. The pH for each polymer was selected to provide the optimum conditons to prevent degradation and enssue stability of nanoparticles.

3.3.1 | Zeta potential of SpAcDEX nanoparticles as a function of HEPES and TRIS concentration

Zeta potential of SpAcDEX particles was studied as a function of buffer concentration of HEPES and TRIS. The results showed that the zeta potential of SpAcDEX particles declined steeply from 14.6 to 4.6 mV on increasing TRIS concentration from 5 to 30 mM (Figure 6). Contrarily, the zeta potential of SpAcDEX particles dispersed in HEPES only marginally declined from 14.5 to 10.6 mV in the concentration range 5–30 mM (Figure 6). In general, a drop in zeta potential of SpAcDEX particles in TRIS/HEPES solution emblems the supression of the electric double layer (EDL) formed at the interface of the Stern layer. Due to the additon of more buffer molecules, there is an increase in ionic concentration of solution. Hence, smaller number of ionic species (building of EDL) are required to screen the surface charge of the particle, in accordance to the models presented by Gouy–Chapman and others.[41–43] However, there is a noticeably less pronounced zeta potential supression in HEPES solution as compared to TRIS uptil 30 mM buffer concentration. This difference in the zeta potential of SpAcDEX in two different buffers illustrates that HEPES through piperazine ring contaitning two nitrogen atoms could contribute to add more positive charge at the SpAcDEX particle surface, thus resisting supression of zeta potential. Further, we also observed that the complete neutralization of the SpAcDEX particles was achieved at 80 and 120 mM of HEPES and TRIS, respectively. This difference could be related to the high valency of sulfonate ions (SO_3^-, HEPES) that could neutralize the surface charge of the particles at a relatively low ionic concentration as compared to TRIS. Other studies have also shown that monovalent and diavalent ions

could alter the zeta potential of nanoparticles by interacting with the Stern layer.[44]

3.3.2 | Zeta potential of AcDEX and PLGA nanoparticles as a function HEPES and TRIS concentration

Zeta potential of AcDEX and PLGA particles was also studied in varying concentrations of HEPES and TRIS at neutral pH (7.2). The results showed that the zeta potential of AcDEX and PLGA dropped as the concentration of HEPES was increased from 5 to 120 mM (Figure 6). In general, we observed a buffer concentration related delcine in zeta potential, which is expected to originate from the supression of the EDL layer in both polymer types; however, we spotted some differences in the zeta potential of polymer particles while they were dispersed in HEPES and TRIS, respectviely.

AcDEX particles expressed zeta potential of –12.9 and –8.2 mV in 5 mM HEPES and TRIS, respectively, which shows that the zeta potenial of AcDEX particles is comparatively less suppressed in HEPES as compared to TRIS. Further, we observed that AcDEX particles exhibited a slightly positive zeta potential (2.1 mV) in 50 mM TRIS (Figure 6). Similarly we observed differences in zeta potential supression of PLGA particles in HEPES and TRIS. PLGA particles showed a zeta potential of –11.4 and –4.6 mV in HEPES and TRIS, respectively, at a buffer concentration of 5 mM. In HEPES, the zeta potential of PLGA particles gradually declined reaching a value of –0.7 mV at 120 mM HEPES concentration. In contrast, zeta potential supression of PLGA was sinficantly less and, in fact, zeta potential more or less remained constant from 10 to 30 mM. Similar to AcDEX, PLGA particles also exhbited small inversion to positive zeta potential (2.1 mV) at 50 mM concentration, probably due to minor absorption of cationic TRIS on PLGA particle surface. Thus, zeta potential supression of PLGA partcles in TRIS particularly at lower buffer concentration (5 mM) appears to emerge from the possible PLGA-TRIS interaction. The amino functional group is likely to interact with the terminal carboxylic functional group of PLGA, thus altering the particles' surface properties. To shed some light on the specific interactions that may occur, we explored this phenomenon with the help of MD simulations.

3.3.3 | Zeta potential of HPMCAS as a function of HEPES and TRIS concentration

HPMCAS particles studied as a function of HEPES and TRIS concentration showed declining zeta potential from –16.5 to –4.1 mV as HEPES concentration was increased from 5 to 80 mM (Figure 6). On the other hand, the zeta potential of HPMCAS-HF remained relatively constant over the wide range of TRIS concentration (5–120 mM). Zeta potential of HPMCAS-HF particles was –6.9 and –6.7 mV in 5 and 120 mM TRIS (Figure 6).

When comparison was made between lower and higher HEPES concentration, HPMCAS-MF particles showed no significant change in zeta potential. In 5 mM HEPES particles expressed –13.6 mV zeta potential, which only marginally increased to –14.7 mV in 120 mM HEPES (Figure 6). Similarly in TRIS, the zeta potential of HPMCAS-MF particles was only slightly decreased from –9.5 to –3.8 mV in TRIS solution of 5 and 120 mM, respectively (Figure 6).

Surprisingly, HPMCAS-LF particles exhibited a rising trend in zeta potential as ionic concentration of HEPES was increased from 5 to 120 mM. 5 mM HEPES particles showed –3.5 mV zeta potential, which soared to –20.7 mV in 120 mM HEPES (Figure 6). In contrast, in TRIS the zeta potential of HMPCAS-LF particles showed a slightly declining trend. The zeta potential of particles was –9.7 mV in 5 mM TRIS, whereas zeta potential decreased to –5.9 mV in 120 mM TRIS (Figure 6).

3.4 | Zeta potential as a function of pH: comparison between HEPES and TRIS

While the charging behavior of acidic and basic groups on the surface of nanoparticles naturally vary as a function of pH, it stands clear that the surface properties of nanomaterials are also highly defined by the surrounding pH,[45] which can be reflected by proper zeta potential measurements. Hence, zeta potential measurements of nanoparticles measured at different pH may also give more insights on the interaction of buffers with nanoparticle surfaces.

3.4.1 | Zeta potential of SpAcDEX particles as a function of pH

We investigated the zeta potential of SpAcDEX particles over pH range 3.5–8.5 both in 25 mM HEPES and TRIS solution. As shown in Figure 7, SpAcDEX particles expressed a higher zeta potential in relatively acidic pH rage (pH 6–3.5) both in HEPES and TRIS solutions, as would be expected from standard zeta potential curves as a function of pH. The amino groups on the spermine chain (linked to SpAcDEX) is slightly basic as shown from the predicted pKa values (8.72–9.51; see Supplementary Information Table S1). Thus, SpAcDEX particles expressing polycationic spermine chain would be protonated under

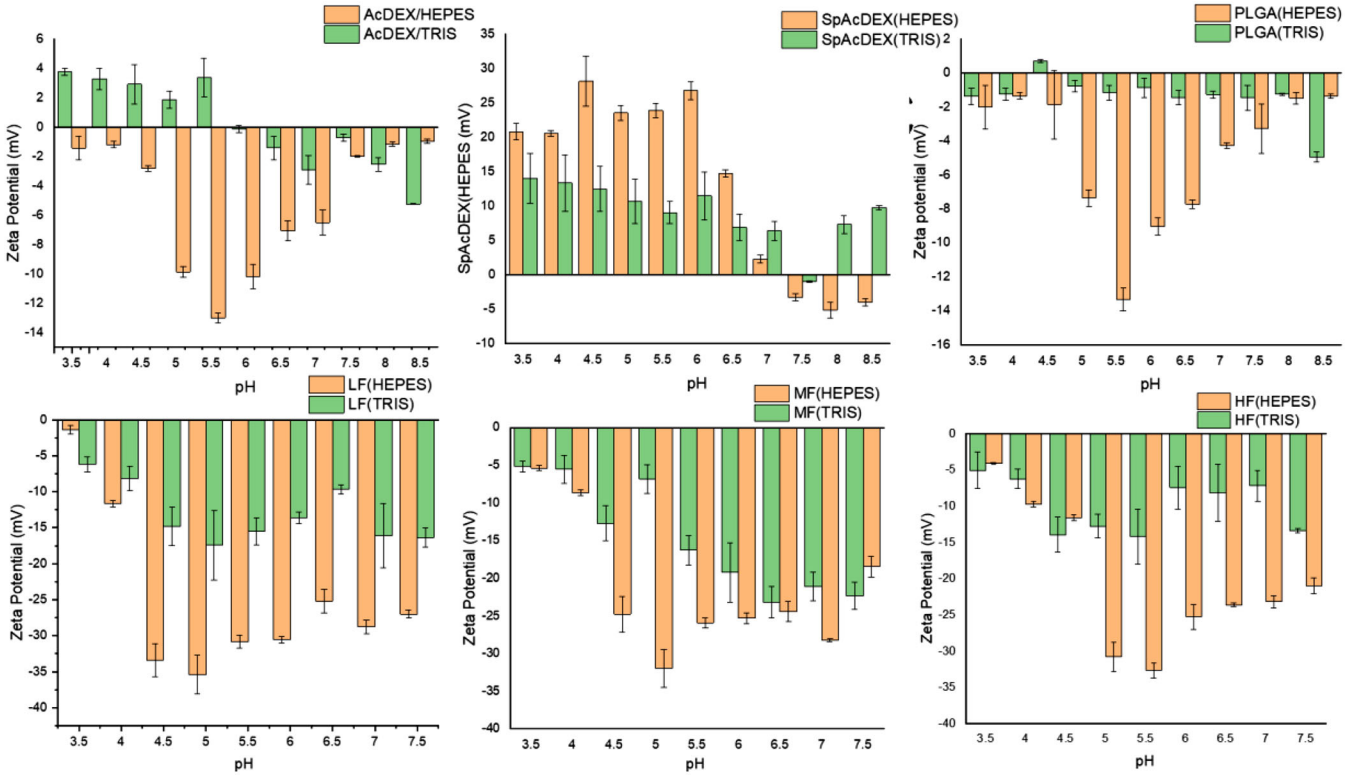

FIGURE 7 Zeta potential of nanoparticles AcDEX, SpAcDEX, PLGA, HPMCAS LF, HPMCAS-MF and HPMCAS-HF, as a function of pH. Particles were dispersed in 25 mM HEPES/TRIS solution adjusted to fixed pH values from 3.5 to 8.5. Zeta potentials were measured with ZetaSizer Nano ZS. Error bars represent standard deviation as calculated from the three measurements

mild acidic conditions, making SpAcDEX particle surface to be more positively charged thus maximizing the zeta potential (positive) value. However, it is important to note that SpAcDEX particles exhibit dissolution below pH 5.5 due to hydrolysis of acetyl groups.[15,46] Hence, zeta potential at pH <5.5 may only represent the existence of monomers of spermine molecules and not the SpAcDEX particles.

The isoelectric point (pH_{iep}) in HEPES and TRIS was achieved at pH 7 and 7.5, respectively (see Figure 7). Further increasing the pH promoted inversion of zeta potential to negative values (−5.1 mV) at pH 8 in HEPES solution, whereas no zeta potential inversion was observed in TRIS solution. This inversion of zeta potential implies that introduction of more hydroxyl ions to make pH alkaline would protonate sulfonic acid moiety of HEPES, thus allowing adsoprtion at the nanoparticle surface due to electrostatic interaction with polycationic spermine chain of SpAcDEX particles. This effect cannot be observed in TRIS due to the lack of a strong acidic functional group. Thus, pH-based investigtion of zeta potential also illustrates that HEPES via sulfonic acid moiety develops electrostatic interaction with SpAcDEX particles and alters zeta potential, which also goes in coherence with the particle-buffer fraction ratio experiment.

3.4.2 | Zeta potential of AcDEX and PLGA particles as a function of pH

AcDEX particles showed maximum zeta potential –13 mV at pH 5.5 in the 25 mM HEPES buffer (Figure 7). However, peak for maximum zeta potential disppeared in TRIS at corresponding pH. AcDEX particles consists of dextran ring, which are conjugated with acetal group that under go hydrolysis at pH 5.5 and below.[47] Thus, molecular rearrangement and ionization of AcDEX particles might increase the surface of particles undergoing hydrolysis, which could be seen as a sharp rise in zeta potential whereas the zeta potential peak in TRIS (Figure 7) is masked in the presence of TRIS, possibly due to the positively charged amino group of TRIS that engages with the hydroxyl group of AcDEX through an ion–dipol interaction.

Similarly, PLGA particles also showed a maximum zeta potential –13.3 mV at pH 5.5 in 25 mM HEPES, which was very close to the maxiumum zeta potential of AcDEX particles in the corresponding buffer and pH (Figure 7). The pKa of PLGA terminal COOH is ca 3 (see Supplementary Information Table S1), which suggests that the carboxylic moiety has a strong acidic nature. Further, according to the predicted pKa curves for PLGA between the pH range

3–8.5, PLGA has a potential to get fully ionized (PLGACOO-) after pH 5. Therefore, above the pKa value (at pH 5.5) PLGA particle surface would become more negatively charged resulting in the maximum zeta potential –13.3 mV (25 mM HEPES). Huang et al. showed that PLGA microspheres degradation starts from the outer crust at the acidic pH.[48] It was proposed in another study that water penetrates the PLGA material and generates free carboxylic groups.[49] Thus, the abrupt rise in zeta potential at critical pH (5.5) may also represent changes in ionization of the PLGA particle surface.

However, in a similar manner to AcDEX, the maximum zeta potential peak also disappeared in TRIS for PLGA particles. This shows that TRIS via its amino end also interacts with the anionic carboxylic terminal group of PLGA, resulting in supresssion of the the zeta potential of PLGA particles specifically at pH 5.5, whereas contrarily in the presence of HEPES, higher zeta potential values were obtained. Thus, both AcDEX and PLGA particles are prone to interact with the amino end of TRIS. To validate the interaction between the functional moities of the buffer molecules and the nanoparticles, and get more molecular insights, we performed MD silmulation studies.

3.4.3 | Zeta potential of HPMCAS particles as a function of pH

As mentioned earlier HPMCAS polymers are produced with the variation of acetyl and succinyl functional moieties, which attributes different soluble properties to the respective polymer grades. HPMCAS-HF contains highest acetyl content (~12%) and lowest succinyl content (~6%) dissolves at pH ≥ 6.8, MF with slightly less acetyl (~9%) and more succinyl content (~11%) shows dissolution at pH ≥ 6 whereas LF with lowest acetyl content (~6%) and highest succinyl (~12%) content dissolves at pH ≥ 5.5. Since the HMPCAS polymer is prone to loose their particle form due to solubility at higher pH, we will focus on the zeta potential data ranging between pH 3.5 and 5.5.

We found that the difference in zeta potential of HPMCAS-HF particles in HEPES and TRIS is neligible from pH 3.5 to 4.5, whereas for HMPCAS-MF and HMPCAS-LF, the difference in zeta potential was insignificant at pH 3.5 and 4.5 (Figure 7). At lower pH, the succinyl moiety would be in depronoated state, as can be seen from its pKa value ca 4 (see Supplementary Information Table S1). Thus, lack of interaction between particles and buffers would not effect the zeta potential of HPMCAS particles in both buffers (HEPES/TRIS) at lower pH (3.5–4/4.5); hence, the zeta potential is expressed in similar fashion.

However, a slight increase in pH (≥4/4.5) would protonate the succinyl moiety, thus favouring interactions between buffers and particles, which in turn may influence zeta potential measurements. We observed that HPMCAS-HF particles showed a prominent shift to –30.8 and –32.7 mV in HEPES (25 mM) at pH 5 and 5.5, whereas in TRIS (25 mM) particles significatly expressed lower zeta potential –12.8 and –14.2 mV at the respective pH values (see Figure 7). HMPCAS-MF particles in turn expressed high zeta potential –24.8, –31.9, and –25.9 mV at pH 4.5, 5, and 5.5 in HEPES (25 mM), respectively (see Figure 7). At the corresponding pH, HMPCAS-MF particles epxressed low zeta potential –12.7, –6.8, and –16.3 mV in TRIS (25 mM), respectively (see Figure 7). Similarly, HPMCAS-LF particles expressed high zeta potential –33.4, –35.4, and –30.8 mV at pH 4.5, 5, and 5.5 in HEPES (25 mM), respectively. At the corresponding pH, HPMCAS-LF particles showed low zeta potential –14.8, –17.4, and –15.5 mV in TRIS (25 mM), respectively (see Figure 7). Hence, higher suppression of zeta potential in TRIS as compared to HEPES was observed in all HPMCAS particles. This advocates that pH by altering buffer/polymers ionization state may significantly increase/decrease interaction between buffers and nanoparticles, whereby stronger interactions may suppress the zeta potential of particles.

3.5 | Predicting molecular interactions with MD simulations

To gain molecular insights into the interactions between the buffer molecules and the studied nanoparticles, we performed MD simulations of each polymer system with either TRIS or HEPES. We first predicted the charges on the buffer molecules and the polymers and then carried out a hydrogen bond analysis to find these polar interactions between the polymer and the buffer molecule.

3.5.1 | Prediction of charges on polymers and buffers

When studying the interaction of polymers with buffer molecules, it is necessary to know the correct ionization state of the polymers and buffer molecules in question. Each simulation system had a total of 20 chains of a particular polymer and 50 molecules of either of the buffers in different proportions at pH 3, 7, and 9 as shown in Table 1. AcDEX does not have any ionizable groups, so it is neutral. SpAcDEX, however, has two predicted ionization states for the spermine chain within the pH range studied (Figure 8). In state 1, all four nitrogen atoms in the spermine chain are protonated while in state 2, three out of the four amine nitrogens are protonated. So, at pH 3, all nitrogen atoms on spermine chain are protonated, and at pH 7 and 9, the

TABLE 1 The number of polymer chains and buffer molecules present in different ionization states at a given pH value in each simulation system

Polymer/buffer	Ionization state	Total no. of chains/molecules		
		pH 3	pH 7	pH 9
AcDEX	No ionization state	20	20	20
SpAcDEX	State 1 (4 protonated N)	20	18	16
	State 2 (3 protonated N)	0	2	4
PLGA	State 1 (all -COOH ionized)	14	20	20
	State 2 (all -COOH unionized)	6	0	0
HPMCAS	State 1 (all -COOH ionized)	0	20	20
(LF, MF, HF)	State 2 (any one -COOH ionized)	10	0	0
	State 3 (all -COOH unionized)	10	0	0
HEPES	State 1 (N on sulphonyl side protonated)	30	15	6
	State 2 ((N on hydroxyl side protonated)	20	15	4
	State 3 (both N deprotonated)	0	20	40
TRIS	State 1 (protonated)	50	48	45
	State 2 (deprotonated)	0	2	5

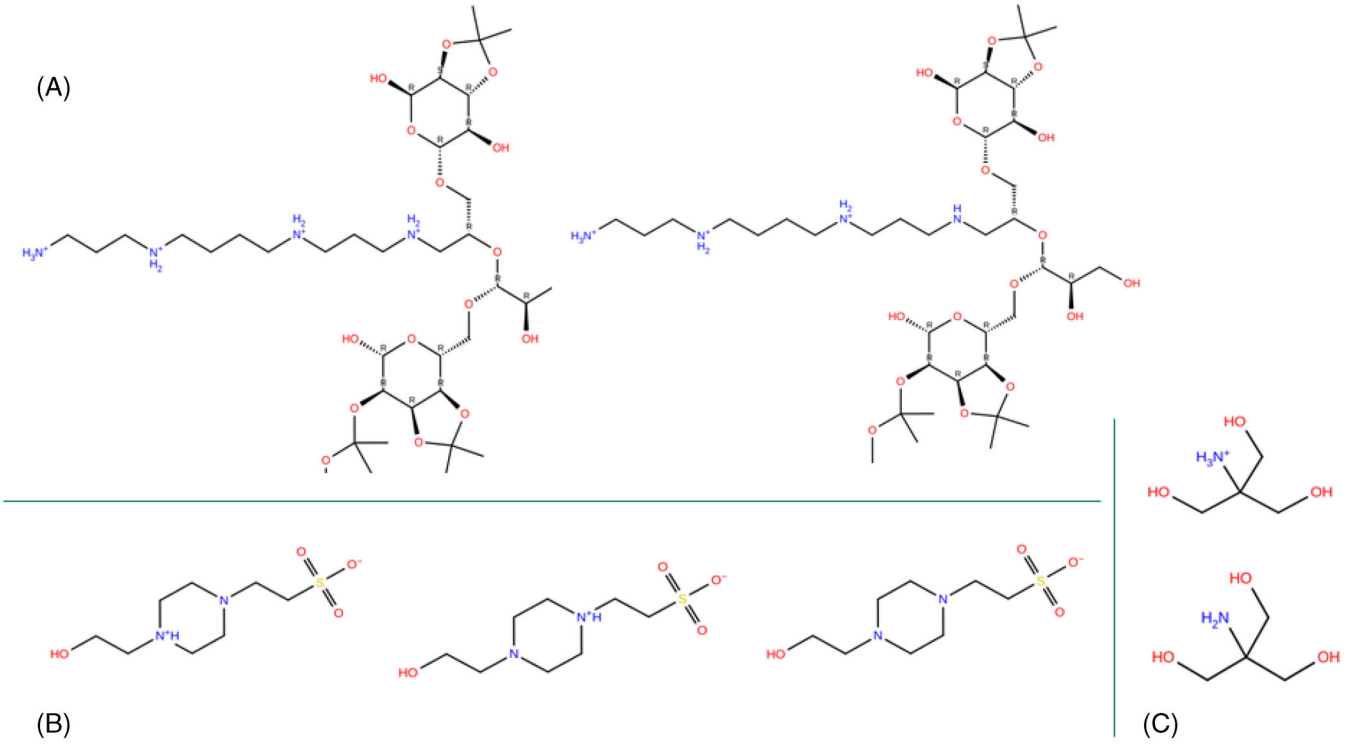

FIGURE 8 Possible ionization states of (A) SpAcDEX polymer, (B) HEPES, and (C) TRIS buffers at pH 5.0–9.0

possibility of having also state 2 present increases as the pH increases. All carboxylic acid groups in PLGA (one group at the end of the polymer chain) and HPMCAS (2, 4 or 6 groups per polymer chain) polymers have a pKa of ca. 3–4 (Supplementary Information, Table S1). Hence, PLGA chains are negatively charged (COO^-) within the pH range 5–9 (state 1) while at pH 3 a few carboxylic acid groups are unionized (COOH; state 2).

Almost half of the HPMCAS polymers chains (LF, MF, and HF) are unionized (state 3) at pH 3. The remaining chains have any one of the carboxylic acids in the ionized form (state 2) (Table 1). At pH 7 and 9, all carboxylic acid groups are fully ionized (state 1). The possible ionization states of HEPES and TRIS molecules were also generated with the help of Epik prediction. States 1 and 2 of HEPES stand for the zwitterionic form where the sulfonic acid

moiety is negatively charged and either of the piperazine nitrogens is protonated. According to the pKa predictions, both piperazine nitrogens have almost the same probability of attracting a proton (predicted pKa values 7.86 and 7.37; cf. experimental pKa 7.55). However, once the other nitrogen is protonated, then the other one cannot be protonated so easily at the same pH as according to the prediction the pKa value of the unprotonated nitrogen drops to ~3.76–5.95. The protonated nitrogen atom in HEPES will start deprotonating at ca. pH 7 and at pH 9 there will be only a small amount of the protonated form available. The amine nitrogen of TRIS buffer stays fully protonated at pH 3 (state 1) and gets deprotonated to only a small extent at pH 7 and 9 as represented in Table 1. The possible tautomers of SpAcDEX and the buffer molecules are shown in Figure 8.

3.5.2 | Hydrogen bonding interactions between polymers and buffers

It is well-known that noncovalent interactions play a significant role in polymer–drug contacts and are responsible for altering various physicochemical properties of polymers. Hence, to study the interactions of the selected buffers with these polymers, we considered the hydrogen bonding interactions as one parameter for understanding the polymer–buffer interactions. The simulations show a clear pattern about these interactions. We observed that the interactions are affected by the pH, size, and the charge of the buffer molecules as well as the nature of the polymer chains. Figure 9 shows an example of a simulation system containing SpAcDEX polymer with HEPES at pH 7.

As a neutral polymer, AcDEX remains unionized at all three different pH values. At acidic and neutral pH, HEPES molecules are in mostly in zwitterionic form and in general favor intermolecular hydrogen bonding with each other (buffer–buffer interaction) as seen in all polymer simulations. Its interactions with AcDEX, however, remain extremely low throughout the simulations, and even at pH 7 and 9, there is no significant difference in the number of H-bond interactions. On other hand, TRIS shows somewhat more H-bond interactions at all three pH values with AcDEX. In SpAcDEX, the protonated spermine chains show strong interactions with HEPES. The number of H-bond interactions increase as the pH rises and the concentration of zwitterionic HEPES molecules decreases (simultaneously giving rise to a bigger proportion of the negatively charged state of the buffer molecule). The number of interactions with TRIS and SpAcDEX remain low and constant at all three pH values. It can be noticed that the buffer and polymer self-interaction patterns remain the same for AcDEX and SpACDEX (Figure 10).

Hydrogen bonding interactions from the MD simulations of PLGA and HPMCAS polymers (LF, MF, and HF) with HEPES and TRIS buffer molecules are presented in Figure 11. TRIS shows more hydrogen bonding interactions with the PLGA polymer than HEPES. The interaction pattern remains relatively similar at all three pH values. The opposite charge on the carboxylate group of PLGA and the protonated amine of TRIS increases the number of hydrogen bonding interactions. This trend can also be seen for the HEPES although the interactions are much less; that is, when the number of positively charged piperazine nitrogens reduces as the pH rises, the interactions decrease between the buffer and the negatively charged polymer). A similar trend in the interactions can be seen for the HPMCAS polymers as well. The lower number of interactions at pH 3 can be explained by the greater number of unionized HPMCAS polymers. It is also seen that the polymer self-interactions are relatively high at pH 3 for HPMCAS-LF and HPMCAS-HF polymers. On other hand, HPMCAS-MF does not show any significant increase in these interactions.

3.5.3 | Radial distribution function (RDF) for charged polymers and buffers

To find the probability of charge distribution around the polymer chains, radial distribution function (RDF) was calculated by measuring the distance between the charge on the polymer chain (the reference) to the positive charge on TRIS and negative charge on HEPES. The RDF curve for SpAcDEX with HEPES and TRIS is shown in Figure 12. As observed from the hydrogen bond interaction analysis, the RDF curve suggests a close presence of HEPES negative charge around the positive charge at the end of the spermine chain of SpAcDEX. As could be seen by the small rise in the RDF curve at 3–4.5 Å, close-range van der Waals and hydrogen bond interactions, and electrostatic interactions, could contribute to the alter zeta potential in the experimental setup. The self-interactions of the zwitterionic HEPES as observed in Figure 10 at pH 3 might be the reason for clustering of HEPES molecules as seen at 7–8 Å. There was no significant presence of the positively charged TRIS molecules observed within 0–8 Å from the SpAcDEX charge.

The RDF curves for PLGA and HPMCAS polymers (LF, MF, and HF grades) are shown below (Figure 13). PLGA and HPMCAS polymers show close interactions with TRIS molecules. Except for the HPMCAS-MF polymer, HEPES does not show considerable charge interactions. At pH 3 HPMCAS polymers with TRIS show a sudden peak at

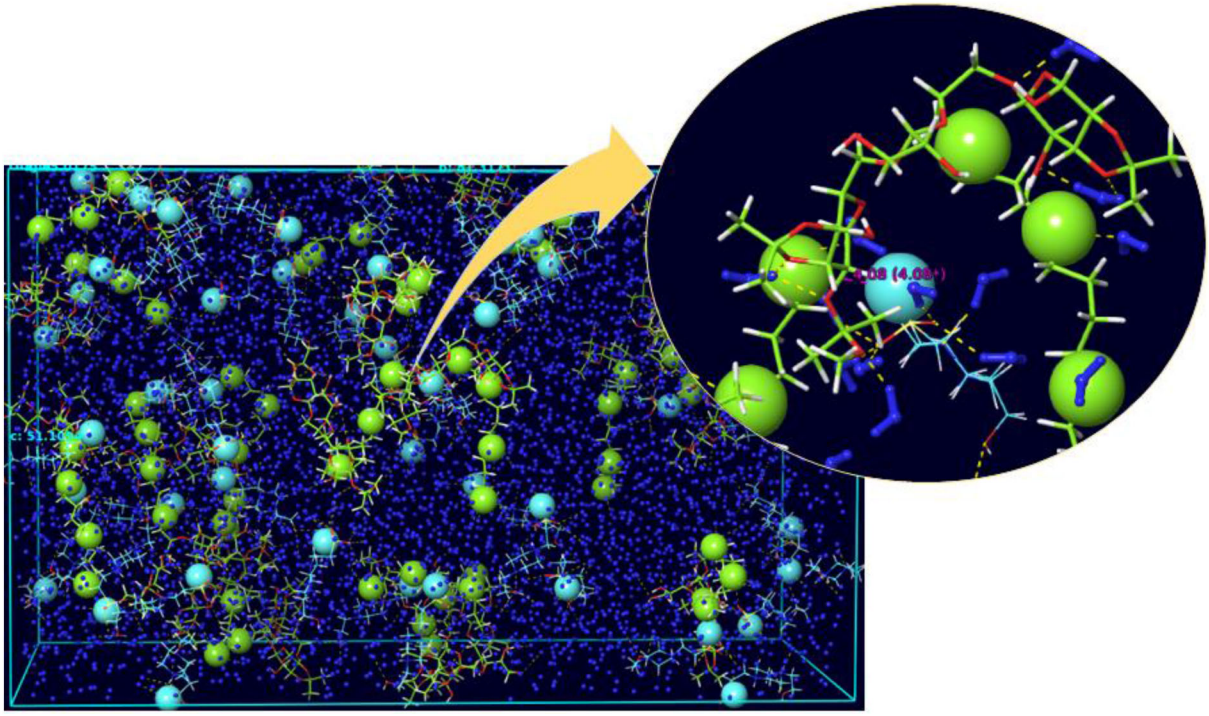

FIGURE 9 The last frame of the 100-ns MD simulation trajectory of SpAcDEX–HEPES–water and enlarged view showing interactions of SpAcDex with HEPES in the presence of water. The charge containing atoms on the spermine chain and HEPES are shown as green and cyan colour spheres, respectively. SpAcDEX polymer is shown in green and buffer molecules in cyan colour sticks; water molecules are shown as single-color blue ball and stick. Atom color code in polymer and buffer molecules: oxygen, red; nitrogen, blue; hydrogen, white; sulphur, yellow. The hydrogen bond interactions are shown as a yellow dashed line, and the distance between two representative charges in Ångströms is labeled purple

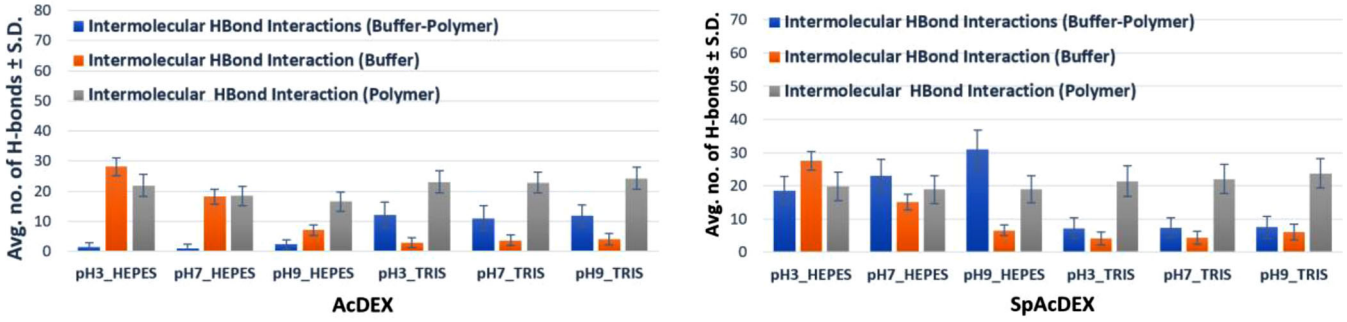

FIGURE 10 Average number of hydrogen bond interactions computed from the 100-ns MD simulations of AcDEX and SpAcDEX polymers with HEPES and TRIS buffer at pH 3, 7, and 9

ca. 3–4 Å that likely comes from an ion–dipole interaction between the positively charged NH^{3+} of TRIS and the unionized carboxylic acid moiety of the polymer. The ionization of the carboxylic acid at higher pH increases the charge-charge interactions between the polymers and the TRIS molecules. It is important to point out that although TRIS shows a high number of hydrogen bonding and electrostatic interactions with these polymers, the magnitude of zeta potential suppression is noticeably less pronounced than in case of the SpAcDEX–HEPES interaction.

It is observed that the addition of spermine chains to AcDEX significantly increases the interactions of HEPES with the polymer and decreases the interactions with TRIS. The RDF curve also confirms that apart from multiple hydrogen bond interactions, short- and long-range electrostatic interactions contribute to stabilizing the SpAcDEX-HEPES contacts. The charge–charge interaction brings the sulfonic acid group of HEPES close to the polymer's spermine chain while the hydroxyl group along with the positively charged piperazine ring of HEPES

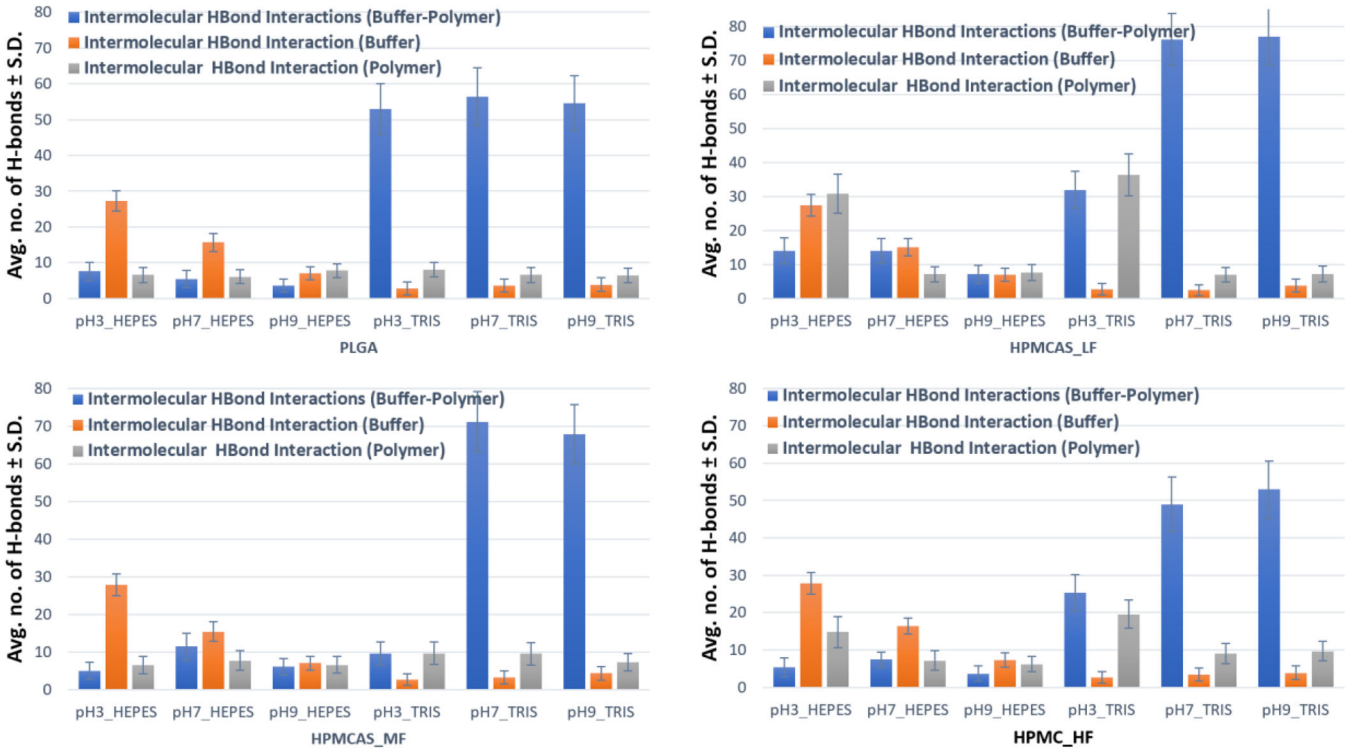

FIGURE 11 The average number of hydrogen bond interactions during the 100-ns MD simulations of PLGA and HPMCAS (LF, MF, and HF) polymers with HEPES and TRIS buffer molecules at pH 3, 7, and 9

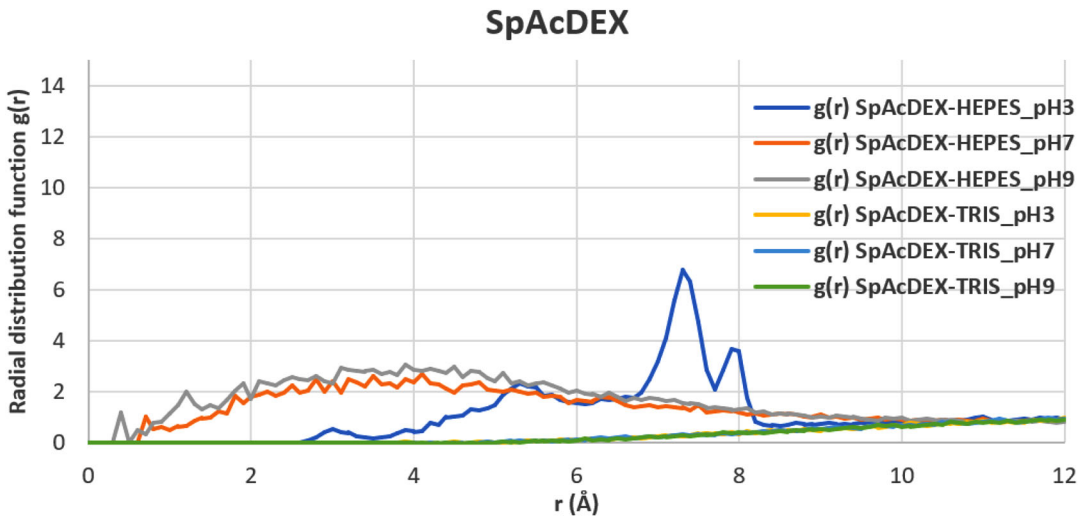

FIGURE 12 The radial distribution function $g(r)$ calculated from the 100-ns MD simulations of SpAcDEX polymers with HEPES and TRIS molecules at pH 3, 7, and 9. The RDF is measured between the positive charge at the end of the spermine chain of SpAcDEX (reference) to the negative charge on HEPES/positive charge on TRIS. The distance r in Å is calculated from the center of the charge and averaged over the simulation trajectory

stays projected outward, which might be the reason for inversion of the zeta potential observed at Fr_L 0.002 (HEPES 25 mM, pH 7.2) as shown in Figure 5. Similar to SpAcDEX-HEPES interaction, TRIS also shows strong hydrogen bonding/electrostatic interactions with PLGA and HPMCAS polymers (LF, MF, and HF), and this can be seen as the suppression of zeta potential. However, these interactions do not lead to inversion of zeta potential due to the absence of a zwitterionic function on TRIS compared to HEPES. This further supports our reasoning

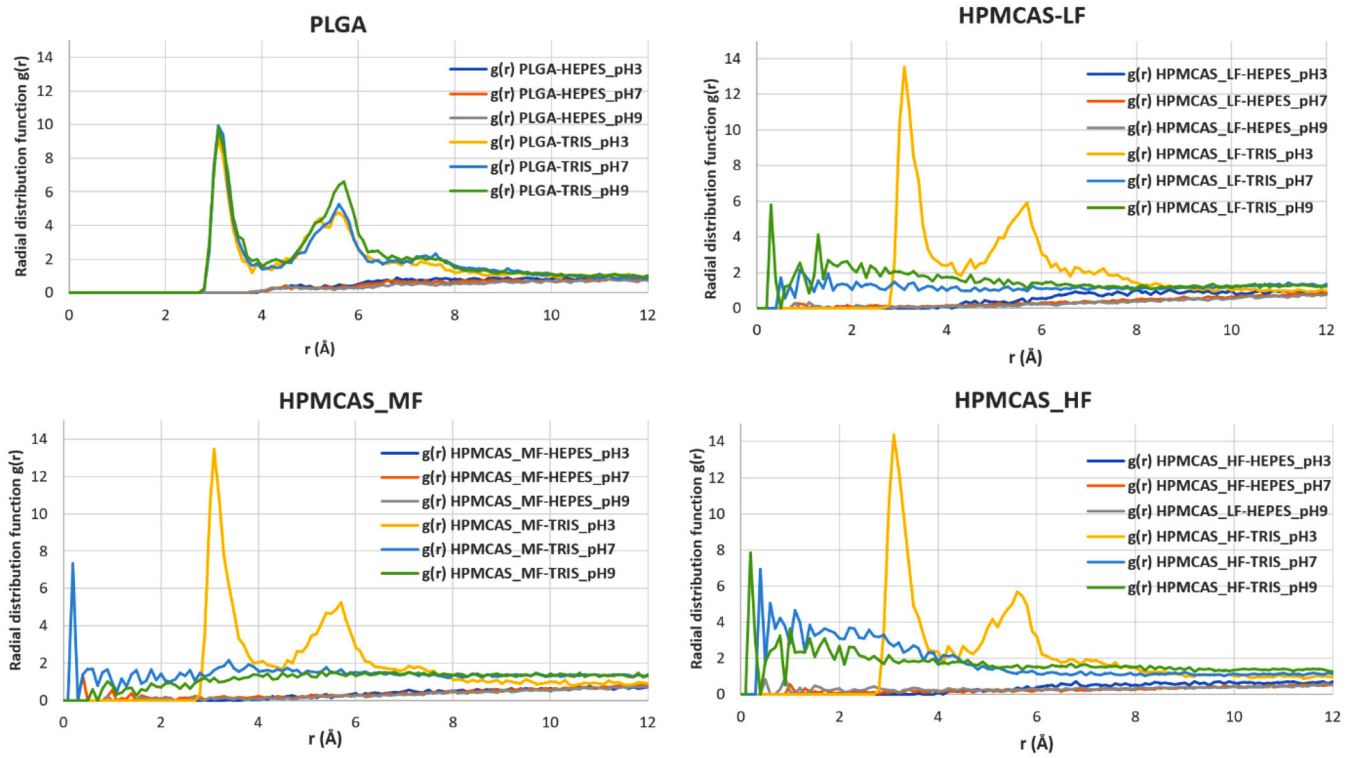

FIGURE 13 The radial distribution function $g(r)$ calculated from the 100-ns MD simulations of PLGA and HPMCAS polymers (LF, MF, and HF) with HEPES and TRIS molecules at pH 3, 7, and 9. For both PLGA and HPMCAS polymers, the RDF is measured between the negatively charged carboxylic acid group (reference) and the negative charge on HEPES/positive charge on TRIS. The distance r in Å is calculated form the center of the charge and averaged over the simulation trajectory

for the cause of the inversion of zeta potential in case of the SpAcDEX-HEPES interaction.

All these findings emphasize the importance of the neglected effect of buffer interactions on the surface properties of nanomaterials. Zeta potential gives an indirect estimate of the charged nanoparticles surface under given conditions, which could be disrupted by counter charged species due to noncovalent interactions. In addition, MD simulations can provide molecular understanding on the interactions of buffers with polymeric nanoparticles. Here we demonstrate that HEPES, by interacting with the spermine chain of SpAcDEX particles, could flip the zeta potential of nanoparticles (Figures 5 and 14), a phenomenon that has not been studied and explored previously. This is affirmed by the higher number of hydrogen bond interactions between SpACDEX and HEPES in our MD simulation study. Likewise, we demonstrate that buffer–particle interaction could also alter (suppress) zeta potential of other polymeric particles. Hence, this study emphasizes the need of careful selection of buffering agents for zeta potential measurements. Further, we also display that fraction ratio (Fr, particles/buffer)-based zeta potential measurement provide a quick approach to access if buffers used are possibly interacting with the particles that could otherwise influence particle characterization.

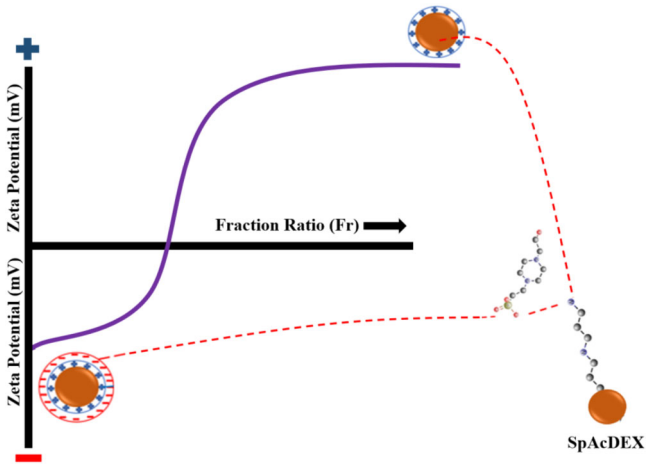

FIGURE 14 Schematic diagram illustrating the shift in zeta potential as fraction ratio (Fr) increases from left to right as indicated by the black arrow. It is shown that at the lowest Fr, particles (SpAcDEX) interact with HEPES via counter charged functional moieties. Spermine amino groups of SpAcDEX form electrostatic/H-bonding interactions with the sulfonic acid moiety of HEPES whereas the carboxylic group of PLGA interacts with the piperazine nitrogen of the HEPES molecule. Thus, zeta potential flipping is observed at a lower Fr whereas zeta potential depicting the true nanoparticle interface is represented best at a higher fraction ratio

Optimum fraction ratio of particles and buffers formulating a pH controlled environment aid to meet conditons to measure zeta potential less influenced by particle–buffer interactions. Therefore, fraction ratio-based zeta potential measurements could give more reliable zeta potential data compared to the single-point zeta potential measurement.

4 | CONCLUSION

Buffers are used to maintain constant pH during evaluation of nanoparticles at specific conditions. Hence, theoretically their role is limited to the extent that there is no association or dissociation with the nanoparticles. This expection can obviously not be held true for all nanoparticles and buffers used as it could be possible that the buffers might start interacting with the surfaces of the nanostructures, altering their physicochemical properties and thus, giving misleading results during evaluation. As there are no clearcut criteria or methods available for the selection of an ideal buffer for given nanoparticle-based formulations, we have here, through experimental investigation and MD simulations, proved that buffer molecules could significantly alter the zeta potential due to strong interaction of the buffer molecules with nanoparticle surfaces. The MD simulations demonstrated that noncovalent interactions, for example, hydrogen bonding and electrostatic interactions of HEPES and TRIS with polymeric nanoparticles might be responsible for the unexpected changes in zeta potential. The shifting of zeta potential during experimental observation at a fixed pH value gives insight about the interaction of nanoparticles with buffer molecules. Moreover, the zeta potential curves obtained in fraction ratio experiments also provide a possibility to discriminate nanoparticles expressing different functional groups (Figure S2, see Supplementary Information). In the light of buffer concentration and pH based investigations of zeta potential, we showed that the basic spermine chain in SpAcDEX can interact with HEPES buffer via hydrogen bonding and charge-charge interactions, leading to zeta potential inversion at a specific ratio of nanoparticles and buffer. On the other hand, TRIS with its basic amino group can freely interact with AcDEX, PLGA, and HMPCAS polymers, which results in unsual zeta potential supression. Therefore, we emphasize the need to carefully select the buffering agent to ensure reliable zeta potential measurements. Zeta potential is inherently a context-dependent property, whereby the conditions must be carefully chosen to provide any useful information. Thus, it is important to presicely manage buffers as well as particle concentrations for informative zeta potential measurements. Based on our study, it seems there is a need to expand the focus of research on a more broad range of buffers to delineate structural features involved in interfering with nanoparticle surface properties. Further, the idea of utilising MD simulations and fraction ratio based evaluation of zeta potential could be explored further to study interactions of small drug molecules with the nanoparticles, whereby the data obtained could be used to predict drug loading and drug release profiles.

ACKNOWLEDGMENTS

We are grateful to the Institute of Biomedicine, University of Turku, for allowing us to use the TEM facility. HARKE Pharma (Germany) is acknowledged for kindly providing the HPMCAS (HF, MF and LF) polymers (Shin-Etsu AQOAT). The Academy of Finland (328933), the Sigrid Jusélius Foundation, and the Toe, Joe and Pentti Borg Memorial Fund are acknowledged for financial support. Biocenter Finland Bioinformatics and Drug Discovery and Chemical Biology networks, CSC IT Center for Science, as well as Prof. Mark Johnson and Dr. Jukka Lehtonen are gratefully acknowledged for the excellent computational infrastructure at Åbo Akademi University. This work is also part of the activities within the strategic research profiling area Solutions for Health at Åbo Akademi University (Academy of Finland, # 336355).

CONFLICT OF INTEREST

The authors declare no competing interests

REFERENCES

1. G. Buckton, *J. Pharm. Pharmacol.* **1995**, *47*, 265.
2. M. Szekeres, E. Tombácz, *Colloids Surfaces A Physicochem. Eng. Asp.* **2012**, *414*, 302.
3. F. S. Dukhovich, M. B. Darkhovskii, E. N. Gorbatova, V. K. Kurochkin, Molecular Recognition: Pharmacological Aspects, Nova Science Publishers, New York, 2004
4. C. Pfeiffer, C. Rehbock, D. Hühn, C. Carrillo-Carrion, D. J. De Aberasturi, V. Merk, S. Barcikowski, W. J. Parak, *J. R. Soc. Interface* **2014**, *11*, 0931
5. T. L. Doane, C. H. Chuang, R. J. Hill, C. Burda, *Acc. Chem. Res.* **2012**, *45*, 317.
6. S. Bhattacharjee, *J. Control. Release* **2016**, *235*, 337.
7. M. Krishnamoorthy, D. Li, A. S. Sharili, T. Gulin-Sarfraz, J. M. Rosenholm, J. E. Gautrot, *Biomacromolecules* **2017**, *18*, 4121.
8. A. Salis, L. Cappai, C. Carucci, D. F. Parsons, M. Monduzzi, *J. Phys. Chem. Lett.* **2020**, *11*, 6805.
9. A. M. Stemig, T. A. Do, V. M. Yuwono, W. A. Arnold, R. Lee Penn, *Environ. Sci. Nano* **2014**, *1*, 478.
10. P.-J. J. Huang, J. Yang, K. Chong, Q. Ma, M. Li, F. Zhang, W. J. Moon, G. Zhang, J. Liu, *Chem. Sci.* **2020**, *11*, 6795.
11. S. Loreto, B. Cuypers, J. Brokken, S. Van Doorslaer, K. De Wael, V. Meynen, *Phys. Chem. Chem. Phys.* **2017**, *19*, 13503.
12. M. J. Mitchell, M. M. Billingsley, R. M. Haley, M. E. Wechsler, N. A. Peppas, R. Langer, *Nat. Rev. Drug Discov.* **2020**, *20*, 101.
13. N. Kamaly, B. Yameen, J. Wu, O. C. Farokhzad, *Chem. Rev.* **2016**, *116*, 2602.

14. E. M. Bachelder, T. T. Beaudette, K. E. Broaders, J. Dashe, J. M. J. Fréchet, *J. Am. Chem. Soc.* **2008**, *130*, 10494.
15. J. L. Cohen, S. Schubert, P. R. Wich, L. Cui, J. A. Cohen, J. L. Mynar, J. M. J. Fréchet, *Bioconjug. Chem.* **2011**, *22*, 1056.
16. R. C. Mundargi, V. R. Babu, V. Rangaswamy, P. Patel, T. M. Aminabhavi, *J. Control. Release* **2008**, *125*, 193.
17. H. Keles, A. Naylor, F. Clegg, C. Sammon, *Polym. Degrad. Stab.* **2015**, *119*, 228.
18. A. L. Sarode, S. Obara, F. K. Tanno, H. Sandhu, R. Iyer, N. Shah, *Carbohydr. Polym.* **2014**, *101*, 146.
19. L. Vorwerg, M. Antonietti, K. Tauer, *Colloids Surfaces A Physicochem. Eng. Asp.* **1999**, *150*, 129.
20. C. J. Van Oss, *Sep. Purif. Rev.* **1975**, *4*, 167.
21. R. Karnik, F. Gu, P. Basto, C. Cannizzaro, L. Dean, W. Kyei-Manu, R. Langer, O. C. Farokhzad, *Nano Lett.* **2008**, *8*, 2906.
22. O. M. H. Salo-Ahen, I. Alanko, R. Bhadane, A. M. J. J. Bonvin, R. V. Honorato, S. Hossain, A. H. Juffer, A. Kabedev, M. Lahtela-Kakkonen, A. S. Larsen, E. Lescrinier, P. Marimuthu, M. U. Mirza, G. Mustafa, A. Nunes-Alves, T. Pantsar, A. Saadabadi, K. Singaravelu, M. Vanmeert, *Process* **2020**, *9*, 71.
23. O. Ben-Zvi, I. Grinberg, A. A. Orr, D. Noy, P. Tamamis, I. Yacoby, L. Adler-Abramovich, *ACS Nano* **2021**, *15*, 6530.
24. M. Zhang, D. Zhang, H. Chen, Y. Zhang, Y. Liu, B. Ren, J. Zheng, *NPJ Comput. Mater.* **2021**, *7*, 1.
25. M. Kanduč, W. K. Kim, R. Roa, J. Dzubiella, *ACS Nano* **2020**, *15*, 614.
26. M. Gaumet, A. Vargas, R. Gurny, F. Delie, *Eur. J. Pharm. Biopharm.* **2008**, *69*, 1.
27. S. Masur, B. Zingsem, T. Marzi, R. Meckenstock, M. Farle, *J. Magn. Magn. Mater.* **2016**, *415*, 8.
28. F. Bernardi, J. D. Scholten, G. H. Fecher, J. Dupont, J. Morais, *Chem. Phys. Lett.* **2009**, *479*, 113.
29. C. Lu, C. Wu, D. Ghoreishi, W. Chen, L. Wang, W. Damm, G. A. Ross, M. K. Dahlgren, E. Russell, C. D. Von Bargen, R. Abel, R. A. Friesner, E. D. Harder, *J. Chem. Theory Comput.* **2021**, 17, 4291.
30. K. J. Bowers, E. Chow, H. Xu, R. O. Dror, M. P. Eastwood, B. A. Gregersen, J. L. Klepeis, I. Kolossvary, M. A. Moraes, F. D. Sacerdoti, J. K. Salmon, Y. Shan, D. E. Shaw, in Proc. 2006 ACM/IEEE Conf. Supercomput. SC'06, ACM Press, New York 2006, p. 84.
31. S. Nosé, *J. Chem. Phys.* **1998**, *81*, 511.
32. S. Nosé, *Mol. Phys.* **2006**, *52*, 255.
33. W. G. Hoover, *Phys. Rev. A* **1985**, *31*, 1695.
34. G. J. Martyna, D. J. Tobias, M. L. Klein, *J. Chem. Phys.* **1998**, *101*, 4177.
35. C. Predescu, A. K. Lerer, R. A. Lippert, B. Towles, J. P. Grossman, R. M. Dirks, D. E. Shaw, *J. Chem. Phys.* **2020**, *152*, 084113.
36. P. Eaton, P. Quaresma, C. Soares, C. Neves, M. P. De Almeida, E. Pereira, P. West, *Ultramicroscopy* **2017**, *182*, 179.
37. K. C. Song, H. S. Lee, I. Y. Choung, K. I. Cho, Y. Ahn, E. J. Choi, *Colloids Surfaces A Physicochem. Eng. Asp.* **2006**, *276*, 162.
38. W. Huang, C. Zhang, *Biotechnol. J.* **2018**, *13*, 1700203.
39. M. von Smoluchowski, *Ann. Phys.* **1906**, *326*, 756.
40. D. C. Henry, *Proc. R. Soc. London. Ser. A, Contain. Pap. a Math. Phys. Character***1931**, *133*, 106.
41. K. G. Marinova, R. G. Alargova, N. D. Denkov, O. D. Velev, D. N. Petsev, I. B. Ivanov, R. P. Borwankar, *Langmuir* **1996**, *12*, 2045.
42. M. Gouy, *J. Phys. Théorique Appliquée* **1910**, *9*, 457.
43. K. B. Oldham, *J. Electroanal. Chem.* **2008**, *613*, 131.
44. S. Dong, Z. Zeng, W. Cai, Z. Zhou, C. Dou, H. Liu, J. Xia, *J. Nanoparticle Res.* **2019**, *21*, 233
45. D. Kowalczyk, I. Kaminska, *J. Mol. Liq.* **2020**, *320*, 114426.
46. T. Bauleth-Ramos, M.-A. Shahbazi, D. Liu, F. Fontana, A. Correia, P. Figueiredo, H. Zhang, J. P. Martins, J. T. Hirvonen, P. Granja, B. Sarmento, H. A. Santos, *Adv. Funct. Mater.* **2017**, *27*, 1703303.
47. K. E. Broaders, J. A. Cohen, T. T. Beaudette, E. M. Bachelder, J. M. J. Fréchet, *Proc. Natl. Acad. Sci. U. S. A.* **2009**, *106*, 5497.
48. B. S. Zolnik, D. J. Burgess, *J. Control. Release* **2007**, *122*, 338.
49. Y. Huang, M. Qi, M. Zhang, H. Liu, D. Yang, *Trans. Nonferrous Met. Soc. China* **2006**, *16*, s293.

AUTHOR BIOGRAPHIES

Wali Inam obtained his Doctor of Pharmacy Degree (Pharm.D) from Hamdard University, Pakistan in 2012. Then he moved to Finland to do Masters in Drug Discovery and Development from University of Turku, Finland. He did his master thesis research work in the Hongbo Zhang research group in 2018. Currently Wali Inam is doing PhD under the supervision of Associate Professor Hongbo Zhang.

Rajendra Bhadane, PhD (Pharm.), is a postdoctoral researcher at the Structural Bioinformatics Laboratory and the Pharmaceutical Sciences Laboratory, Åbo Akademi University, Turku, Finland. He obtained his doctoral degree in Pharmacy from the Suresh Gyan Vihar University, Jaipur in 2018, India. He has worked in Dr. Outi M. H. Salo-Ahen's computer-aided drug design group since September 2019. He was an Acting Head of Divine College of Pharmacy 2016–2019 and held a position of an Assist. Professor in Pharmacy Institutes affiliated to the University of Pune 2007–2016. He has published 11 peer-reviewed articles.

Rukiye Nur Akpolat graduated from the Erciyes University Faculty of Pharmacy in 2019. During her education, she had the opportunity to do a 6-month internship at Prof. Hongbo Zhang's Microfluidics laboratory. During her visit, she investigated zeta potential of polymer nanoparticles. She is currently working as the chief pharmacist in the Corum Alaca Public Hospital at Turkey.

Rifahul Abrar Taiseer, Quality control scientist working for Amneal Pharmaceutical LLC, USA with extensive experience in pharmaceutical chemistry and biological sciences. Prior to joining Amneal, Mr. Rifahul has worked in Pharmaceutical science laboratory of Åbo Akademi University. He also worked on prostate cancer development pathways in molecular biology lab

of University of Bedfordshire, UK. Mr. Rifahul is a registered pharmacist in his home country Bangladesh.

Prof. Sergey Filippov is a Leverhulme professor at School of Pharmacy, Reading University, UK. Prof. Filippov's main research interests are dynamic light scattering, small-angle X-ray and neutron scattering, and isothermal titration calorimetry in application to self-assembling systems in soft matter including polymers, lipids, surfactants. He is also interested in the application of physical methods to study drug delivery systems.

Adjunct Professor (docent) Outi M. H. Salo-Ahen, DSc (Pharm.), is a University Lecturer in Pharmacy at the Åbo Akademi University, Pharmaceutical Sciences Laboratory, Turku, Finland. She obtained her doctoral degree in Pharmacy from the University of Kuopio in 2006, Finland. As a postdoc she worked in Prof. Dr. Rebecca Wade's Molecular and Cellular Modeling group at the Heidelberg Institute for Theoretical Studies in Germany for three years. She then continued her research first in the Structural Bioinformatics Laboratory of the Biochemistry unit at the Åbo Akademi University (ÅAU), Turku, Finland (2009–2014) and then in the Pharmacy unit of ÅAU (2014–2015). She was an acting Professor in Pharmacy at ÅAU 2015–2020. Currently, she leads a research group that focuses on computer-aided drug design and computational pharmaceutics. She has published 38 peer-reviewed articles (h = 20, i10 = 26, 1517 citations; Google Scholar 4/2/2022).

Jessica M. Rosenholm, DSc (Tech.), is Professor in Pharmaceutical Development at the Åbo Akademi University, Pharmaceutical Sciences Laboratory, Turku, Finland. She obtained her doctoral degree in Physical Chemistry in 2008 and adjunct professorship (docent) in Biomedical Nanotechnology in 2013 from the same university. In 2009–2010 she spent a postdoctoral period at the Nano Biomedical Research Centre, Med-X Research Institute, Shanghai Jiao Tong University in China. Upon returning to Finland in 2010, she established and is currently heading the BioNanoMaterials research group that focuses mostly on nanomedicines but is also involved in exploring other types of novel drug delivery technologies such as 3D printing. To date, she has published 186 peer-reviewed articles and book chapters (h = 44, i10 = 113, 8256 citations; Google Scholar 4/2/2022).

Hongbo Zhang graduated his PhD from the Faculty of Pharmacy, University of Helsinki in December 2012 and did his Postdoc in Harvard University between 2014–2016. He has a multidisciplinary background in pharmacy, nanotechnology, microfluidics, precision medication, molecular biology; and he knows the world leading technologies. He has published more than 130 papers with google citation of 5300, H-index of 45. He established his research group "Functional Materials for Medicine" in 2016 in Åbo Akademi University and now he is a Tenure Track Associate Professor at the Pharmaceutical Sciences Laboratory within the Solutions for Health strategic research profiling area at ÅAU.

SUPPORTING INFORMATION

Additional supporting information may be found in the online version of the article at the publisher's website.

How to cite this article: W. Inam, R. Bhadane, R. N. Akpolat, R. A. Taiseer, S. K. Filippov, O. M. H. Salo-Ahen, J. M. Rosenholm, H. Zhang, *VIEW*. **2022**, 20210009.
https://doi.org/10.1002/VIW.20210009